Inorganic Chemistry

Article

pubs.acs.org/IC

Rollover Cyclometalation with 2-(2′-Pyridyl)quinoline

Antonio Zucca,*[,†] Diletta Cordeschi,[†] Luca Maidich,[†] Maria Itria Pilo,[†] Elisabetta Masolo,[†] Sergio Stoccoro,[†] Maria Agostina Cinellu,[†] and Simona Galli[‡]

[†]Dipartimento di Chimica e Farmacia, Università degli Studi di Sassari, via Vienna 2, 07100 Sassari, Italy

[‡]Dipartimento di Scienza e Alta Tecnologia, Università dell'Insubria, via Valleggio 11, 22100 Como, Italy

Supporting Information

ABSTRACT: Rollover cyclometalation of 2-(2′-pyridyl)quinoline, L, allowed the synthesis of the family of complexes [Pt(L-H)(X)(L′)] and [Pt(L*)(X)(L′)][BF_4] (X = Me, Cl; L′ = neutral ligand), the former being the first examples of Pt(II) rollover complexes derived from the ligand L. The ligand L* is a C,N cyclometalated, N-protonated isomer of L, and can also be described as an abnormal-remote pyridylene. The corresponding [Pt(L-H)(Me)(L′)]/[Pt(L*)(Me)(L′)]$^+$ complexes constitute an uncommon Brønsted−Lowry acid−base conjugated couple. The species obtained were investigated in depth through NMR and UV−vis spectroscopy, cyclic voltammetry, and density functional theory (DFT) methods to correlate different chemico-physical properties with the nature of the cyclometalated ligand (e.g., L vs bipy or L* vs L) and of the neutral ligand (DMSO, CO, PPh_3). The crystal structures of [Pt(L-H)(Me)(PPh_3)], [Pt(L-H)(Me)(CO)] and [Pt(L*)(Me)(CO)][BF_4] were determined by X-ray powder diffraction methods, the latter being the first structure of a Pt(II)-based, protonated, rollover complex to be unraveled. The isomerization of [Pt(L*)(Me)(PPh_3)]$^+$ in solution proceeds through a retro-rollover process to give the corresponding adduct [Pt(L)(Me)(PPh_3)]$^+$, where L acts as a classical N,N chelating ligand. Notably, the retro-rollover reaction is the first process, among the plethora of Pt−C bond protonolysis reactions reported in the literature, where a Pt−C(heteroaryl) bond is cleaved rather than a Pt−C(alkyl) one.

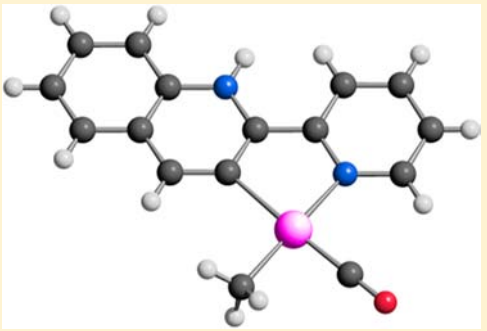

INTRODUCTION

The chemistry of cyclometalated compounds is of great current interest because of the wide range of potential applications they may have in many areas, such as organic synthesis, homogeneous catalysis, photochemistry, and design of advanced materials and biologically active agents.[1]

An emerging class of cyclometalated compounds consists of the so-called "rollover complexes", derived from bidentate chelating ligands for which partial decomplexation and internal rotation of the ligand allow an inactivated, remote C−H bond to interact with the metal and give rise to a cyclometalated species (Scheme 1). Such behavior, called "rollover" cyclometalation, is still rather rare.[2]

Much effort has been devoted to shed light into the mechanism of the rollover process. The fundamental mechanistic difference between "classical" and "rollover" cyclometalation lies in the nature of the starting adduct. Rollover cyclometalation originates by definition from a chelated adduct, and the crucial point is the internal rotation of the ligand, which occurs before the C−H bond activation. In the case of platinum(II), the first studies on the topic showed the nucleophilic nature of the metal ion in the course of the C−H bond activation.[3] Successive studies in the gas phase demonstrated a clear preference for an oxidative-addition/reductive-elimination mechanism for platinum,[4] whereas σ-bond metathesis is favored for nickel. In the case of palladium, the preferred mechanism depends on the nature of the anionic ligands coordinated to the metal ion.[4]

The most studied ligand in this context is 2,2′-bipyridine (bipy),[5] but the family of rollover complexes comprises other bidentate heterocyclic ligands, such as 2,2′:6′,2″-terpyridine,[6] 2-(2′-thienyl)pyridines,[7] pyrazolylmethanes,[8] *N*-(2-pyridyl)-7-azaindole,[9] and even 2-phenylpyridines.[10] The peculiarity of rollover complexes derives from the presence of an uncoordinated donor atom, usually a nitrogen or a sulfur, which may influence the reactivity and properties of the whole complex. The growing interest in this emerging field is evidenced by the publication of a very recent review dedicated to this topic.[2] Worthy of note, rollover complexes have been recently found to promote C−C bond formation in the gas phase by activation of chloromethanes[11] and by dehydrosulfurization of thioethers.[12] In addition, rollover cyclometalation pathways have found catalytic applications in the hydroarylation of alkenes and alkynes with 2,2′-bipyridines and 2,2′-biquinolines,[13] and in the transformation of 3-alkynyl and 3-alkenyl-2-arylpyridines into 4-azafluorene compounds.[14] Moreover, insertion reactions in the metal−carbon bond have been successfully used for the synthesis of C(3) substituted bipyridines,[15] while double rollover metalation on the

Received: April 12, 2013
Published: June 14, 2013

   dx.doi.org/10.1021/ic400908f | *Inorg. Chem.* 2013, 52, 7717−7731

Scheme 1. Rollover Cyclometalation

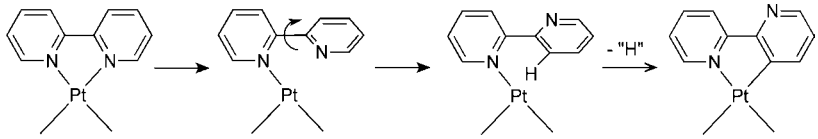

bipyridine ligand has afforded polymeric organometallic species[3a] or bimetallic complexes where the metal centers are connected by a highly delocalized planar system.[16]

Rollover derivatives of 2,2′-bipyridine may be compared to the analogous derivatives of 2-phenylpyridine (Chart 1), with

Chart 1

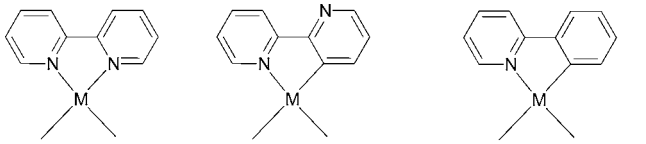

the striking difference that the formally anionic, deprotonated rollover 2,2′-bipyridine is no more a spectator ligand, but may be an active participant in the course of the chemical transformations of the complex, through, for example, coordination or protonation. In particular, protonation of the uncoordinated nitrogen atom allows the synthesis of uncommon cationic complexes which may be regarded either as mesoionic species,[17] or abnormal pyridylenes.[18] These compounds may convert into the corresponding Pt(N,N) adducts through a "retro-rollover" reaction.[19] The reversibility of the rollover process, found in ruthenium,[20] rhodium,[21] and platinum complexes,[10,12] is extremely attractive, offering, in principle, the possibility to design catalytic cycles based on "rollover"/"retro-rollover" paths, employing the bipy/bipy-H ligands as a hydrogen atom reservoir/acceptor system.

As for the more common cyclometalated species, also in the case of rollover compounds the properties of the complexes may be modulated on the basis of the nature of the cyclometalated ligand. Rollover cyclometalation may indeed create a highly delocalized system. Thus, following our continuous efforts in the comprehension of the behavior of cyclometalated[22] and rollover[16,23] derivatives of platinum(II), we have decided to investigate a more delocalized ligand, such as 2-(2′-pyridyl)-quinoline, L (Scheme 2). The latter, compared

Scheme 2. 2-(2′-Pyridyl)quinoline, L, with the Atom Number Labeling Scheme Used Throughout the Paper

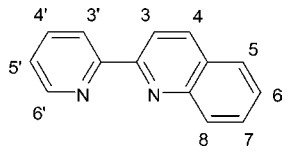

to 2,2′-bipyridine, possesses an additional fused ring, potentially imparting different electronic and steric properties, and has been investigated until now only by classical coordination means: examples available in the literature involve iron,[24] rhodium,[25] platinum,[26] and gold.[27]

The higher electronic delocalization of quinoline compared to pyridine deserves a few comments: because of the additional condensed ring, the quinoline nitrogen is expected to be more basic, having the possibility to delocalize the positive charge, after protonation, on a larger area. Actually, other effects contribute to the basicity, such as solvation and steric congestion. In particular, the peri-effect,[28] generating repulsion between the N−H hydrogen and the adjacent C−H one in the N-protonated quinoline, lowers the stability of this species, so that the basicity scale is quinoline < pyridine < isoquinoline (pK_b = 9.15, 8.83, 8.54, respectively; Chart 2).[29]

Chart 2

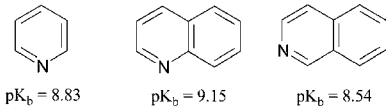

On the whole, the electronic effects for 2-(2′-pyridyl)-quinoline are not trivial and may furnish, together with the augmented steric hindrance, additional interesting potentialities with respect to 2,2′-bipyridine.

We report here the first example of an air- and moisture-stable Pt(II) rollover complex containing 2-(2′-pyridyl)-quinoline, a coherent picture of which is provided by means of NMR (^{1}H, ^{13}C, 2D-COSY, NOE-1D experiments), IR and electronic spectroscopy, as well as cyclic voltammetry. The versatile chemistry of this species is further described in terms of its behavior toward different acids and in substitution reactions. Finally, an example of spontaneous retro-rollover reaction[19] is reported and described in detail. This reaction, which may have considerable potential applications in catalysis,[2] proceeds through internal protonolysis and cleavage of a Pt−C(heteroaryl) rather than a Pt−C(alkyl) bond. To the best of our knowledge, this is the only case, among the plethora of Pt−C bond protonolysis reactions reported in the literature, where a Pt−C(heteroaryl) bond is cleaved rather than a Pt−C(alkyl) one.[30]

It is worth remembering that protonolysis of M−CH_3 bonds, considered as the microscopic reverse reaction of the activation of alkane C−H bonds, has been the subject of extensive mechanistic investigations.[31]

EXPERIMENTAL SECTION

Materials and Methods. *Cis*-[Pt(Me)$_2$(DMSO)$_2$] was synthesized according to the literature.[32,33] All the solvents were purified and dried according to standard procedures.[34] Elemental analyses were performed with a Perkin-Elmer elemental analyzer 240B. Infrared spectra were recorded with a FT-IR Jasco 480P in solution or using Nujol mulls. ^{1}H, ^{13}C{^{1}H}, and ^{31}P{^{1}H} NMR spectra were recorded with a Varian VXR 300 or a Bruker Avance III 400 spectrometer. Chemical shifts are given in ppm relative to internal TMS for ^{1}H and ^{13}C{^{1}H}, and to external 85% H_3PO_4 for ^{31}P{^{1}H}. *J* values are given in hertz (Hz). NOE difference, 2D-COSY, 2D-NOESY and ^{13}C apt (attached proton test) experiments were performed by means of standard pulse sequences.

dx.doi.org/10.1021/ic400908f | Inorg. Chem. 2013, 52, 7717−7731

UV−vis spectra were recorded on a Hitachi U-2010 spectrophotometer. Cyclic voltammetric tests were performed using an Autolab PGSTAT12 (Ecochemie) potentiostat/galvanostat interfaced with a PC under GPES software, employing a single-compartment three-electrode cell, at room temperature, under Ar atmosphere, at a potential scan rate of 100 mV s^{-1}. A 2 mm diameter Pt disk electrode (CH Instruments) was used as working electrode, an aqueous Ag/AgCl (Amel) with suitable salt bridge was adopted as the reference electrode, and a graphite rod was the auxiliary electrode. All the experiments were carried out in CH_2Cl_2 (Sigma-Aldrich, anhydrous, ≥99.8%) using 0.1 M tetraethylammonium hexafluorophosphate ($TEAPF_6$, Sigma-Aldrich, for electrochemical analysis, ≥99.0%) as supporting electrolyte, with sample concentration about 2×10^{-3} M.

Computational Details. All calculations were carried out using the Firefly QC package,[35] which is partially based on the GAMESS (US)[36] source code, using the hybrid PBE0 functional developed by Perdew, Burke and Ernzerhof[37,38] and implemented in the hybrid form by Adamo and Barone.[39] Ahlrichs and co-workers[40] def2-SVP basis set, as found in the EMSL basis set library,[41] were used for all lighter atoms (H, C, N, O, S, and P), while for platinum the same basis set was integrated with an effective core potential (ECP) removing 60 core electrons. Convergence criteria were tightened compared to the default ones: an SCF cycle was considered converged if the density change, in absolute value, between two subsequent iterations was less than 10^{-6}; the geometry was considered converged if the largest component of the gradient, in hartree $bohr^{-1}$, was less than 10^{-6}.

Frequency analysis at the same level of theory (PBE0/def2-SVP) and with the same convergence parameters was carried out for all equilibrium geometries to check their nature on the potential energy surface (PES). The calculations on all complexes showed no imaginary frequencies in the output thus confirming that they are true minima.

Time-dependent density functional theory (TD-DFT),[42,43] as implemented in the Firefly program, was used to calculate the lowest 30 excited states having singlet multiplicity.

Preparations. *Synthesis of 2-(2′-Pyridyl)quinoline, L. Method A.* 2-(2′-Pyridyl)quinoline was prepared according to literature methods[44] from quinoline-N-oxide. The first step of the synthesis requires the isolation of 2-cyano-quinoline, which was prepared by the reaction, at 0 °C, of quinoline-N-oxide (4.00 g, 27.5 mmol), $(CH_3)_2NCOCl$ (3.17 g, d = 1.168 g/mL, 29.0 mmol) and $(CH_3)_3SiCN$ (3.9 mL, 2.92 g, d = 0.744, 29.0 mmol) in CH_2Cl_2 (Yield 65%). 2-(2′-Pyridyl)-quinoline was obtained from 2-cyano-quinoline through co-cyclotrimerization of acetylene in the presence of Bönnemann catalyst (Co(cp)COD), in toluene at 120 °C, with a 30% yield.

Method B. 2-(2′-pyridyl)quinoline was prepared by cyclization between *o*-aminobenzaldehyde and 2-acetylpyridine, according to references 24 and 45. Yield 45%.

^{1}H NMR (ppm, $CDCl_3$): 7.36 (ddd, 1H, $H_{5'}$, J_{H-H} = 7.5, 4.8, 1.2 Hz); 7.55 (ddd, 1H, H_6, J_{H-H} = 8.4, 6.7 Hz); 7.75 (ddd, 1H, H_7, J_{H-H} = 8.2, 6.7 Hz); 7.84−7.90 (m, 2H, $H_{3',4'}$); 8.18 (d, 1H, H_5, J_{H-H} = 8.5 Hz); 8.28 (d, 1H, H_4, J_{H-H} = 8.6 Hz); 8.56 (d, 1H, H_3, J_{H-H} = 8.6 Hz); 8.65 (d, 1H, H_8, J_{H-H} = 8.2 Hz); 8.74 (ddd, 1H, $H_{6'}$, J_{H-H} = 5.6 Hz).

*Synthesis of [Pt(L-H)(Me)(DMSO)], **2a**.* To a solution of *cis*-$[Pt(Me)_2(DMSO)_2]$ (100 mg, 0.262 mmol) in acetone (30 mL), 54 mg of 2-(2′-pyridyl)quinoline, L (0.262 mmol) were added under vigorous stirring. The solution was heated to 50 °C for 4 h, then it was evaporated to a small volume and treated with *n*-hexane. The precipitate formed was filtered off, washed with *n*-hexane and vacuum pumped to give the analytical sample as a yellow solid. Yield 90%. Anal. (%) calc for $C_{17}H_{18}N_2OSPt$: C = 41.38, H = 3.68, N = 5.68. Found C = 41.27, H = 3.43, N = 5.56. Mp 150 °C (dec). ^{1}H NMR (ppm, $CDCl_3$): 0.82 (s sat, 3H, CH_3−Pt, $^2J_{Pt-H}$ = 82.0 Hz); 3.29 (s sat, 6H, CH_3(DMSO), $^3J_{Pt-H}$ = 18.3 Hz); 7.43 (ddd, 1H, J_{H-H} = 7.2, 5.5, 1.4 Hz, $H_{5'}$); 7.47 (ddd, 1H, J_{H-H} = 8.3, 6.8, 1.3 Hz, H_6); 7.60 (td, 1H, H_7, J_{H-H} = 8.3, 6.8, and 1.5 Hz); 7.79 (d, 1H, H_5, J_{H-H} = 8.3 Hz); 8.01 (td, 1H, $H_{4'}$, J_{H-H} = 7.8 Hz); 8.03 (d, 1H, H_8, J_{H-H} = 8.3 Hz); 8.41 (s sat, 1H, H_4, $^3J_{Pt-H}$ = 60.4 Hz); 8.62 (d, 1H, $H_{3'}$, J_{H-H} = 7.9 Hz); 9.82 (ddd sat, 1H, $H_{6'}$ J_{H-H} = 5.6, 1.6, 0.8 Hz, $^3J_{Pt-H}$ = 14.2 Hz). ^{13}C NMR (ppm, $CDCl_3$): −13.07 (Pt-CH_3, J_{Pt-C} = 766.1 Hz); 43.77 (DMSO, J_{Pt-C} = 41.9 Hz); 122.46 (J_{Pt-C} = 23.2 Hz); 125.19 (J_{Pt-C} = 10.7 Hz); 126.37; 127.42; 127.88; 129.20; 129.23 (J_{Pt-C} = 64.5 Hz); 138.36; 139.26 (J_{Pt-C} = 89.0 Hz); 140.80 (Pt−C, J_{Pt-C} = 1090 Hz); 146.32; 150.45; 161.75 (Cq, J_{Pt-C} = 52.4 Hz); 166.09 (Cq, J_{Pt-C} = 27.9 Hz).

When the reaction is followed at room temperature in acetone-d_6, a mixture of complexes **1** and **2a** is observed in solution by means of ^{1}H NMR.

Complex **1**, selected ^{1}H NMR data: 1.23 (s sat, 3H, CH_3, $^2J_{Pt-H}$ = 86.7 Hz); 1.16 ppm (s sat, 3H, CH_3, $^2J_{Pt-H}$ = 88.9 Hz); 8.90 (dd sat, 1H, $H_{6'}$, $^3J_{Pt-H}$ = 24.4 Hz).

*Synthesis of [Pt(L-H)(Me)(PPh_3)], **2b**.* To a solution of **2a** (95.7 mg, 0.121 mmol) in CH_2Cl_2 (25 mL), 32.0 mg of PPh_3 (0.121 mmol) were added under vigorous stirring. The solution was stirred for 1 h, then concentrated to a small volume and treated with *n*-hexane. The precipitate formed was filtered off and washed with *n*-pentane to give the analytical sample as a yellow solid. Yield 95%. m.p.: 201−205 °C. Anal. (%) calcd for $C_{33}H_{27}N_2PPt$: C = 58.49, H = 4.02, N = 4.13; found C = 58.23, H = 3.95, N = 3.83. ^{1}H NMR (ppm, $CDCl_3$): 0.86 (d sat, 3H, CH_3−Pt, $^3J_{P-H}$ = 7.5 Hz, $^2J_{Pt-H}$ = 83.1 Hz); 6.73 (m, 1H, $H_{5'}$); 7.38−7.46 (m, 11H, aromatics); 7.58 (m, 1H, H_7); 7.76−7.87 (m, 9H, aromatics); 8.02 (d, 1H, H_8, J_{H-H} = 8.0 Hz); 8.64 (d sat, 2H, H_4+$H_{3'}$, $^4J_{P-H}$ = 6.0 Hz, $^3J_{Pt-H}$ = 53.6 Hz). ^{31}P NMR (ppm, $CDCl_3$): 33.4 (s sat, PPh_3, J_{Pt-P} = 2236 Hz).

*Synthesis of [Pt(L-H)(Me)(CO)], **2c**.* CO was bubbled into a solution of **2a** (86.0 mg, 0.178 mmol) in CH_2Cl_2 (20 mL) at room temperature for 2 h. The solution was concentrated to a small volume and treated with *n*-pentane. The precipitate formed was filtered off, washed with *n*-pentane, and vacuum pumped to give the analytical sample as a dark-yellow solid. Yield 85%. Anal. (%) calcd for $C_{16}H_{12}N_2OPt$ C = 43.34, H = 2.73, N = 6.32, found C = 43.37, H = 2.67, N = 5.94. m.p.: 180 °C. ^{1}H NMR (ppm, $CDCl_3$): 1.29 (s sat, 3H, CH_3−Pt, $^2J_{Pt-H}$ = 85.9 Hz); 7.37 (ddd, 1H, $H_{5'}$, J_{H-H} = 7.2, 5.4, 1.5 Hz); 7.50 (ddd, 1H, H_6, J_{H-H} = 8.1 Hz); 7.61 (ddd, 1H, H_7, J_{H-H} = 8.2, 1.5 Hz); 7.79 (dd, 1H, H_5, J_{H-H} = 8.2 Hz); 8.01 (m, 1H, H_8); 8.03 (dt, 1H, $H_{4'}$, J_{H-H} = 7.7, 1.6 Hz); 8.46 (s sat, 1H, H_4, $^3J_{Pt-H}$ = 53.7 Hz); 8.61 (dd, 1H, H_3, J_{H-H} = 7.7 Hz); 8.71 (dd sat, 1H, $H_{6'}$, J_{H-H} = 5.4 Hz, $^3J_{Pt-H}$ = 18 Hz). IR (CH_2Cl_2, ν_{max}/cm^{-1}): 2057 s (CO); (Nujol, ν_{max}/cm^{-1}): 2053 s (CO).

*Synthesis of [Pt(L-H)(Cl)(DMSO)], **4a**.* To a solution of complex **2a** (100 mg, 0.203 mmol) in acetone (25 mL), 2.0 mL of HCl 0.1 M (0.203 mmol) and 0.2 mL of DMSO (2.8 mmol) were added under vigorous stirring. The mixture was stirred for 8 h, then complex **4a** was extracted with CH_2Cl_2 (3 × 10 mL), dried with Na_2SO_4, filtered, and concentrated to a small volume. Addition of *n*-pentane produced a precipitate that was filtered off, washed with *n*-pentane and vacuum pumped to give the analytical sample as a yellow solid. Yield 65%. Anal. (%) calcd for $C_{16}H_{15}ClN_2OSPt$: C = 37.39, H = 2.94, N = 5.45. Found C = 37.03, H = 2.71, N = 5.07. m.p.: 200 °C. ^{1}H NMR (ppm, $CDCl_3$): 3.71 (s sat, 6H, CH_3 (DMSO), $^3J_{Pt-H}$ = 24.0 Hz); 7.48 (m, 2H, $H_{5'}$+H_6); 7.63 (m, 1H, H_7); 7.81 (d, 1H, H_5, J_{H-H} = 8.3 Hz); 8.00 (dd, 1H, H_8, J_{H-H} = 7.8 Hz); 8.05 (t, 1H, $H_{4'}$, J_{H-H} = 7.8 Hz); 8.55 (d, 1H, $H_{3'}$, J_{H-H} = 8.3 Hz); 9.02 (s sat, 1H, H_4, $^3J_{Pt-H}$ = 46.3 Hz); 9.71 (d sat, 1H, $H_{6'}$, J_{H-H} = 4.8 Hz, $^3J_{Pt-H}$ = 33.3 Hz). Assignments based on 2D- COSY and NOESY spectra.

*Synthesis of [Pt(L-H)(Cl)(PPh_3)], **4b**.* To a solution of **4a** (50.0 mg, 0.097 mmol) in CH_2Cl_2 (25 mL), 30.7 mg of PPh_3 (0.116 mmol) were added under stirring. The solution was stirred for 4 h, then concentrated to a small volume and treated with diethyl ether. The precipitate formed was filtered off and washed with diethyl ether to give the analytical sample as a yellow solid. Yield 94%. Anal. (%) calcd for $C_{32}H_{24}ClN_2PPt$: C = 55.06, H = 3.47, N = 4.01. Found C = 55.28, H = 3.71, N = 3.88. m.p.: 195 °C. ^{1}H NMR (ppm, $CDCl_3$): 6.86 (d, 1H, J_{H-H} = 8.3 Hz); 7.16−7.21 (m, 2H); 7.35−7.54 (m, 12H); 7.80−7.90 (m, 6H, aromatics); 8.05 (t, 1H, J_{H-H} = 7.9 Hz); 9.98 (d sat, 1H, $H_{6'}$, $^3J_{Pt-H}$ = 30 Hz). ^{31}P NMR (ppm, $CDCl_3$): 22.4 (s sat, PPh_3, J_{Pt-P} = 4288 Hz).

*Synthesis of [Pt(L-H)(Cl)(CO)], **4c**.* To a solution of **4a** (50.0 mg, 0.089 mmol) in CH_2Cl_2 (20 mL) CO was bubbled for 6 h at room temperature. The crude mixture was then filtered, concentrated to a small volume and treated with *n*-hexane. The precipitate formed was filtered, washed with *n*-hexane and vacuum pumped to give the

dx.doi.org/10.1021/ic400908f | Inorg. Chem. 2013, 52, 7717−7731

analytical sample as a yellow solid. Yield 65%. m.p.: 150 °C (dec). Anal. (%) calc for $C_{15}H_9ClN_2OPt$: C = 38.85, H = 1.96, N = 6.04. Found C = 38.50, H = 1.87, N = 5.83. ^{1}H NMR (ppm, $CDCl_3$): 7.54 (m, 2H, $H_{5'}$+H_6); 7.71 (m, 2H); 8.02 (d, 1H, H_5, J_{H-H} = 8.3 Hz); 8.12 (m, 2H, $H_{3'}$+$H_{4'}$); 8.53 (m, 1H, H_8); 9.58 (d sat, 1H, $H_{6'}$, J_{H-H} = 5.4 Hz, $^3J_{Pt-H}$ = 33 Hz). IR (Nujol, ν_{max}/cm^{-1}): 2106 s (CO).

Synthesis of [Pt(L)(Me)(DMSO)][BF$_4$],* ***5a-BF$_4$.*** To a solution of **2a** (50 mg, 0.101 mmol) in CH_2Cl_2 (25 mL), 41.3 mg of [18-crown-6-H_3O][BF_4] (0.111 mmol) were added under vigorous stirring. After 1 h the solution was filtered, concentrated to a small volume and treated with diethyl ether. The precipitate formed was filtered off, washed with diethyl ether, and vacuum pumped to give the analytical sample as a green-yellow solid. Yield 80%. Anal. (%) calc for $C_{17}H_{19}BF_4N_2OSPt$: C = 35.15, H = 3.29, N = 4.82. Found C = 35.02, H = 3.58, N = 4.63. m.p.: 140 °C (dec). ^{1}H NMR (ppm, $CDCl_3$): 0.85 (s sat, 3H, CH_3–Pt, $^2J_{Pt-H}$ = 81.3 Hz); 3.33 (s sat, 6H, CH_3 (DMSO), $^3J_{Pt-H}$ = 20.3 Hz); 7.69 (m, 1H); 7.76 (m, 1H); 7.95–8.02 (m, 2H, aromatics); 8.31 (m, 1H); 8.53 (d, 1H, J_{H-H} = 8.1 Hz); 8.95 (d, 1H, H_8, J_{H-H} = 7.9 Hz); 9.02 (s sat, 1H, H_4, $^3J_{Pt-H}$ = 63 Hz); 10.0 (d sat, 1H, $H_{6'}$, J_{H-H} = 5.2 Hz, $^3J_{Pt-H}$ = 13.2 Hz); 13.9 (broad, 1H, N–H). IR (Nujol, ν_{max}/cm^{-1}): 3280, 1058, s br (BF_4^-).

Synthesis of [Pt(L)(Me)(PPh$_3$)][BF$_4$],* ***5b-BF$_4$.*** To a solution of **2b** (24.4 mg, 0.36 mmol) in CH_2Cl_2 (15 mL) 13.4 mg of [18-crown-6-H_3O][BF_4] (0.036 mmol) were added. After 2 h, the mixture was concentrated to a small volume and treated with Et_2O to form a precipitate. The solid was filtered off, washed with Et_2O and vacuum-pumped to give the analytical sample as a yellow solid. Yield 90%. Anal. (%) calc for $C_{33}H_{28}BF_4N_2PPt$: C = 51.78; H = 3.69; N = 3.66; found: C = 51.96; H = 3.57; N = 3.49. ^{1}H NMR (ppm, $CDCl_3$): 0.91 (s sat, 3H, $^3J_{P-H}$ = 7.2 Hz, $^2J_{Pt-H}$ = 82 Hz); 7.04 (t, 1H, J_{H-H} = 6.4 Hz, $H_{5'}$); 7.40–7.56 (m, 9H); 7.70–7.84 (m, 7H); 7.92–8.11 (m, 3H); 8.21 (td, J_{H-H} = 9.0, 1.2 Hz, $H_{4'}$); 8.53 (d, 1H, J_{H-H} = 8.7 Hz, $H_{3'}$); 9.35 (d sat, 1H, $^4J_{P-H}$ = 5.6 Hz, $^3J_{Pt-H}$ = 55.2 Hz, H_4); 9.91 (d, 1H, J_{H-H} = 8.1 Hz, H_8); 13.79 (s, br, 1H, NH). ^{31}P NMR (ppm, $CDCl_3$): 32.0 (s sat, PPh_3, J_{Pt-P} = 2507 Hz).

Synthesis of [Pt(L)(Me)(CO)][BF$_4$],* ***5c-BF$_4$.*** To a solution of **2c** (17.7 mg, 0.040 mmol) in CH_2Cl_2 (15 mL) 14.7 mg of [18-crown-6-H_3O][BF_4] (0.040 mmol) were added. After 2 h, the mixture was concentrated to a small volume and treated with Et_2O to form a precipitate. The solid was filtered off, washed with Et_2O and vacuum-pumped to give the analytical sample as a yellow solid. Yield 85%. Anal. (%) calc for $C_{16}H_{13}BF_4N_2OPt$: C = 36.18; H = 2.47; N = 5.27; found: C = 36.04; H = 2.58; N = 5.11. ^{1}H NMR (ppm, $CDCl_3$): 1.36 (s sat, 3H, CH_3, $^2J_{Pt-H}$ = 84.0 Hz); 7.75 (m, 1H); 7.85 (m, 1H); 8.06 (m, 2H); 8.47 (m, 1H); 8.60 (d, 2H, J_{H-H} = 7.9 Hz); 8.98 (d, 1H, $H_{6'}$, J_{H-H} = 4.8 Hz); 9.10 (d, 1H, J_{H-H} = 9.0 Hz); 9.17 (s, 1H, H_4). IR (Nujol, cm^{-1}): 3340 m, 2079 vs, 1074 vs, br.

Synthesis of [Pt(L)(Cl)(PPh$_3$)][BF$_4$],* ***6-BF$_4$.*** To a solution of **4b** (25.0 mg, 0.036 mmol) in CH_2Cl_2 (15 mL) 13.4 mg of [18-crown-6-H_3O][BF_4] (0.036 mmol) were added. After 2 h, the mixture was concentrated to a small volume and treated with Et_2O to form a precipitate. The solid was filtered off, washed with Et_2O and vacuum-pumped to give the analytical sample as a yellow solid. Yield 90%. Anal. (%) calc for $C_{32}H_{25}BClF_4N_2PPt$: C = 48.91; H = 3.21; N = 3.56. Found: C = 48.60; H = 3.19; N = 3.66. ^{1}H NMR (ppm, $CDCl_3$): 7.05 (d, 1H, J_{H-H} = 8.1 Hz); 7.43–7.66 (m, 10H, aromatics); 7.80–7.86 (m, 8H, aromatics); 7.90 (m, 1H); 8.39–8.48 (m, 2H); 9.02 (d, 1H, $H_{3'}$), 10.14 (m sat, 1H, $H_{6'}$, $^3J_{Pt-H}$ =25 Hz), 13.9 (s broad, 1H, NH). ^{31}P NMR (ppm, $CDCl_3$): 20.1 (s sat, PPh_3, J_{Pt-P} = 4143 Hz).

Synthesis of [Pt(L)(Me)(PPh$_3$)][BF$_4$], ***7-BF$_4$.*** To a solution of **2b** (6.8 mg, 0.01 mmol) in CD_2Cl_2 (1.0 mL) 3.6 mg of [18-crown-6-H_3O][BF_4] (0.01 mmol) were added. The reaction was followed through ^{1}H and ^{31}P NMR spectroscopy. After 2 days, the conversion into the adducts [Pt(L)(Me)(PPh_3)]$^+$ was complete (almost 100% conversion). Selected NMR data (ppm, $CDCl_3$):

7c, P *cis* to N(quinoline) (minor species, ca. 44%) ^{1}H: 0.96 (3H, d sat, CH_3, $^3J_{P-H}$ = 3.2 Hz, $^2J_{Pt-H}$ = 70 Hz), 7.65 (d, 1H, H_6, J_{H-H} = 5.6 Hz), 8.85 and 8.76 (AB system, 2H, H_3 + H_4, J_{A-B} = 8.5 Hz). ^{31}P NMR: 17.1 (J_{Pt-P} = 4410 Hz).

7t, P *trans* to N(quinoline) (main species, ca. 56%) ^{1}H: 0.72 (3H, d sat, CH_3, $^3J_{P-H}$ = 4.7 Hz, $^2J_{Pt-H}$ = 74 Hz), 8.72 and 8.69 (AB system, 2H, H_3 + H_4, J_{A-B} = 8.5 Hz), 8.94 (m broad, 1H, $^4J_{P-H}$ ≈ J_{H-H} ≈ ca. 4.5–5.0 Hz, $^3J_{Pt-H}$ = 34 Hz, $H_{6'}$). ^{31}P NMR: 15.2 (J_{Pt-P}= 4449 Hz).

Other ^{1}H NMR signals: 8.91 (d, 1H, J_{H-H} = 8.5 Hz), 8.80 (d, 1H, J_{H-H} = 7.9 Hz), 8.47 (m, 1H), 8.42 (t, 1H, J_{H-H} = 8.7 Hz), 8.22 (d, 1H, J_{H-H} = 7.8 Hz), 8.09 (d, 1H, J_{H-H} = 8.1 Hz), 7.84–7.21 (m, PPh_3), 7.01 (m, 1H), 6.83 (m, 1H).

X-ray Powder Diffraction Structural Analysis. Polycrystalline samples of compounds **2b**, **2c** and **5c-BF$_4$**, not containing single crystals of suitable quality, were deposited in the hollow of an aluminum sample-holder equipped with a quartz zero-background plate.[46] For all the species, diffraction data were collected by means of overnight scans in the 2θ range of 5–105°, with steps of 0.02°, on a Bruker AXS D8 Advance diffractometer, equipped with Ni-filtered Cu–Kα radiation (λ = 1.5418 Å), with a Lynxeye linear position-sensitive detector, and with the following optics: primary beam Soller slits (2.3°), fixed divergence slit (0.5°), receiving slit (8 mm). The generator was set at 40 kV and 40 mA. Standard peak search, followed by indexing through the Singular Value Decomposition approach[47] implemented in TOPAS-R,[48] allowed the detection of the approximate unit cell parameters of all the species. The space groups were assigned on the basis of the systematic absences. Prior to structure solution, unit cells and space groups were checked by means of Le Bail refinements. Structure solutions were performed by the simulated annealing technique, implemented in TOPAS, employing rigid, idealized models: in the case of **2b** and **5c-BF$_4$**, a rigid group was defined comprising the whole Pt(II) complex (completed, for **5c-BF$_4$**, by a rigid group describing the counterion). As for **2b**, two rigid groups were defined, comprising the PPh_3 moiety and the residual portion of the complex, respectively. Average values, retrieved by analyzing similar moieties present in the Cambridge Structural Database, were assigned to the bond parameters defining the stereochemistry at the metal ions, the ligands, and the counterion. The rollover nature of the complexes was established in all the cases by NMR. Thus, a rigid body comprising a *C,N*-chelating ligand was adopted. Nonetheless, the possibility of having a CH_3 moiety *trans* to the carbon atom, not to the nitrogen one, was investigated at the stage of structure solution. In all the cases, the geometry suggested by NMR resulted in structural models with lower figures of merit, which were thus adopted for the final structure refinements.

A heavy preferred orientation along [1 0 1] affected the diffractogram of **2c**: at the structure solution stage, the mere introduction of a correction in the March-Dollase formulation did not allow to reach convergence to a sensible structural model. A reasonable model was obtained only minimizing the preferred orientation by acquiring XRPD data on a batch of **2c** admixed with a dispersing, amorphous material (flour). For the refinement stage, to avoid the contribution of flour to the diffractogram, preferred orientation was hampered by side-loading **2c** onto the sample-holder. The final refinements were carried out by the Rietveld method, maintaining the rigid bodies introduced at the solution stage, but allowing the ligand to depart from planarity. The background was modeled by a Chebyshev polynomial function. One, isotropic thermal parameter was assigned to the metal atoms (B_M) and refined; lighter atoms were given a B_{iso} = B_M + 2.0 Å^2 thermal parameter. Final Rietveld refinement plots are shown in Supporting Information, Figure S1. Fractional atomic coordinates are supplied in the Supporting Information as CIF files. X-ray crystallographic data in CIF format have been deposited at the Cambridge Crystallographic Data Center as supplementary publications no. CCDC 933079 (**2b**), CCDC 933080 (**2c**) and CCDC 933081 (**5c-BF$_4$**). Copies of the data can be obtained free of charge on application to the Director, CCDC, 12 Union Road, Cambridge, CB2 1EZ, U.K. (Fax: +44–1223–335033; e-mail: deposit@ccdc.cam.ac.uk or http://www.ccdc.cam.ac.uk).

Crystal Data for [Pt(L-H)(PPh$_3$)(Me)], ***2b.*** $C_{33}H_{27}N_2PPt$, M_r = 677.64, triclinic, $P\bar{1}$, a = 10.6066(4) Å, b = 12.1023(5) Å, c = 12.8774(5) Å, α = 98.863(3)°, β = 94.042(2)°, γ = 55.167(2)°, V = 1340.3(1) Å^3; Z = 2; ρ_{calc} = 1.7 g cm^{-3}; F(000) = 664; μ(CuKα) =

dx.doi.org/10.1021/ic400908f | Inorg. Chem. 2013, 52, 7717–7731

Chart 3

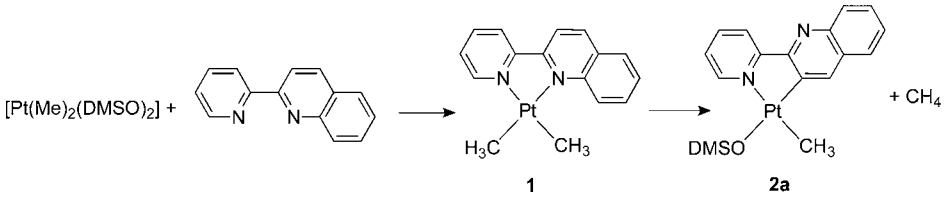

101.6 cm^{-1}. R_p, R_{wp}, and R_{Bragg}, 0.045, 0.059, and 0.034, respectively, for 45 parameters.

Crystal Data for [Pt(L-H)(CO)(Me)], ***2c.*** $C_{16}H_{12}N_2OPt$, M_r = 443.36, monoclinic, $P2_1$, a = 17.123(2) Å, b = 8.3068(6) Å, c = 9.7524(9) Å, β = 96.502(6)°, V = 1378.2(2) $Å^3$; Z = 4 (Z' = 2); ρ_{calc} = 2.1 g cm^{-3}; $F(000)$ = 416; μ(CuKα) = 182.9 cm^{-1}. R_p, R_{wp}, and R_{Bragg}, 0.078, 0.122, and 0.082, respectively, for 58 parameters.

Crystal Data for [Pt(L)(Me)(CO)][BF$_4$],* ***5c -BF$_4$.*** $C_{16}H_{13}BF_4N_2OPt$, M_r = 538.18, monoclinic, $P2_1/n$, a = 20.195(2) Å, b = 10.7569(7) Å, c = 7.7571(5) Å, β = 100.703(4)°, V = 1655.8(2) $Å^3$; Z = 4; ρ_{calc} = 2.2 g cm^{-3}; $F(000)$ = 1000; μ(CuKα) = 157.2 cm^{-1}. R_p, R_{wp}, and R_{Bragg}, 0.052, 0.073, and 0.035, respectively, for 56 parameters.

RESULTS AND DISCUSSION

Synthesis and Characterization of the Rollover Complex [Pt(L-H)(Me)(DMSO)], 2a. The ligand 2-(2′-pyridyl)quinoline, L (Scheme 2), was synthesized following two different routes: (a) from quinoline N-oxide via 2-CN-pyridine and co-cyclotrimerization with acetylene in the presence of Bönneman catalyst [CpCo(COD)];[49] b) by cyclization between *o*-aminobenzaldehyde, obtained in situ by reduction of *o*-nitrobenzaldehyde with iron, and 2-acetylpyridine (see the Experimental Section).[24,45]

Despite its similarity with bipy, one of the most widely studied ligands in coordination chemistry,[50] 2-(2′-pyridyl)-quinoline has been the subject of only a few papers, where it acts exclusively as a bidentate N,N donor.[24,27] Compared to 2,2′-bipyridine, L possesses an additional fused ring, potentially able to furnish supplementary electronic and steric properties. In the case of platinum(II), only the adducts [Pt(L)X_2] (X = Cl, Br, I) are presently known, synthesized from the corresponding bisbenzonitrile complexes [Pt(PhCN)$_2X_2$].[26]

By contrast, we report here that the reaction of the electron rich platinum(II) derivative [Pt(Me)$_2$(DMSO)$_2$] follows a different route, depending on the reaction conditions. As a matter of fact, the reaction between [Pt(Me)$_2$(DMSO)$_2$] and L in acetone at room temperature yields the adduct [Pt(L)-(Me)$_2$], **1**, which rapidly converts into the corresponding rollover complex [Pt(L-H)(Me)(DMSO)], **2a** (Chart 3). To the best of our knowledge, the latter is the first example of a rollover complex containing the ligand L.

The overall reaction from [Pt(Me)$_2$(DMSO)$_2$] to **2a** was followed by means of ^{1}H NMR spectroscopy in deuterated acetone at room temperature (see Scheme 2 for the atom numbering). The spectra show the conversion of [Pt-(Me)$_2$(DMSO)$_2$] into [Pt(L)(Me)$_2$] (**1**) (molar ratio 5:1 after approximately 1 min) and of the latter into [Pt(L-H)(Me)(DMSO)] (**2a**), according to the pathway [Pt-(Me)$_2$(DMSO)$_2$] → [Pt(L)(Me)$_2$] → [Pt(L-H)(Me)-(DMSO)] (Chart 3). The two processes have comparable rates, so that complex **2a** is already present in solution before complete conversion of [Pt(Me)$_2$(DMSO)$_2$] into **1**. Indeed, after 20 min, [Pt(Me)$_2$(DMSO)$_2$], [Pt(L)(Me)$_2$], and [Pt(L-H)(Me)(DMSO)] are present in solution in a 10:5:1 molar ratio.

Complex **1** is easily detected in solution by the presence of two coordinated methyl groups (δ 1.23 ppm, $^2J_{Pt-H}$ = 86.7 Hz; δ 1.16 ppm, $^2J_{Pt-H}$ = 88.9 Hz) with Pt−H coupling constants in line with N−Pt−Me *trans* arrangements. The $H_{6'}$ proton, as expected, is slightly deshielded and coupled to ^{195}Pt (δ 8.90 ppm, $^3J_{Pt-H}$ = 24.4 Hz), this evidence confirming the coordination of the pyridine ring.

Unfortunately, the simultaneous presence in solution of the starting compounds, [Pt(Me)$_2$(DMSO)$_2$] and L, of the intermediate adduct **1** and of the rollover complex **2a** does not allow the isolation of **1** as a pure product.

Simultaneously to the first step of the reaction (the displacement of the DMSO ligands by L), the rollover reaction takes place: the quinoline nitrogen (i.e., the most hindered one) moves away from the metal, allowing rotation of the quinoline moiety so that the initially remote C_3−H bond may approach the metal and, likely through an oxidative-addition/reductive-elimination pathway, gives room-temperature C−H bond activation and rollover cyclometalation. The process is irreversible because of the elimination of methane.

This mechanism was already proposed for the rollover metalation of 2,2′-bipyridines on the basis of NMR and kinetic data,[3] even though no evidence for a Pt(IV) species was provided by NMR, and was subsequently confirmed by mechanistic studies in the gas phase.[51]

Complete conversion of the intermediate adduct into the rollover species occurs, faster, in acetone at 50 °C, and complex **2a** may be isolated in high yield in the solid state and characterized.

The C−H bond activation is regiospecific: by contrast with the symmetric 2,2′-bipyridine, in the present case two geometric isomers are possible, but only one is formed, that is, that derived from the activation of the C−H bond in the quinoline ring, having an N−Pt−CH_3 *trans* arrangement. No activation in the pyridine ring is observed. This is in line with previously reported data,[3b] which indicate that rollover cyclometalation is extremely sensitive to steric factors. It should be noted that the same reaction with 2,2′-bipyridine, which gives the corresponding complex [Pt(bipy-H)(Me)(DMSO)], **3**,[5] occurs only under harsher conditions (toluene, reflux); the different behavior of the two ligands could be ascribed to the presence of the condensed ring on one of the pyridine rings of L; the acceleration of the reaction may be thus attributed mainly to steric factors, which destabilize the adduct **1**, but electronic factors, which can contribute to stabilize the transition state, may be active as well and cannot be completely ruled out.

Complex **2a** was thoroughly characterized by means of analytical and spectroscopic methods. In the absence of a structural characterization, a detailed NMR study (^{1}H, ^{13}C, 2D-COSY, NOE-1D experiments) confirmed the proposed molecular structure (Chart 4). The ^{1}H NMR spectrum confirms metalation, showing only nine aromatic protons. In particular, the formation of the C(3)−Pt bond is demonstrated

dx.doi.org/10.1021/ic400908f | Inorg. Chem. 2013, 52, 7717−7731

Chart 4

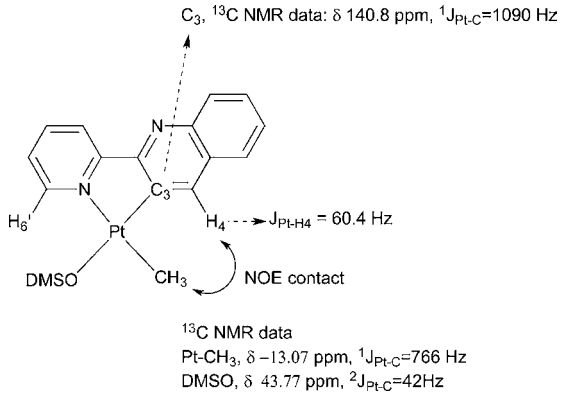

by the lack of the signal of the H_3 proton, by the signal of the H_4 proton (a singlet with satellites at 8.41 ppm, $^3J_{Pt-H}$ = 60.4 Hz) and by the signal, in the ^{13}C NMR spectrum, of the quaternary metalated C(3) (140.8 ppm), the $^1J_{Pt-C}$ coupling constant value (1090 Hz) being in agreement with a strong Pt−C(sp^2) bond.

The coordination of the pyridine nitrogen is confirmed by the deshielding of the $H_{6'}$ signal, at 9.82 ppm, typical of a pyridine ring coordinated to Pt in *cis* to a DMSO moiety,[5] and, mostly, by the coupling ^{195}Pt−$H_{6'}$: the $^3J_{Pt-H}$ value, 14.2 Hz, is in line with a N−Pt−C *trans* arrangement.

The coordination sphere of the metal center is completed by the methyl group and by a DMSO moiety, which show ^1H and ^{13}C NMR signals in agreement with a methyl coordinated in *trans* to a pyridine nitrogen (^1H: δ 0.82 ppm, $^2J_{Pt-H}$ = 82 Hz; ^{13}C: δ −13.1 ppm, $^1J_{Pt-C}$ = 766 Hz), and a DMSO ligand in *trans* to an sp^2 carbon (^1H: δ 3.29 ppm, $^3J_{Pt-H}$ = 18.3 Hz; ^{13}C: δ 43.8 ppm, $^2J_{Pt-C}$ = 42 Hz).

The geometry of **2a** was also ascertained by a series of NOE-1D NMR spectra, which show, inter alia, an NOE contact between the coordinated methyl group and the H_4 proton. Finally, a COSY experiment enabled us to fully assign the signals in the ^1H NMR spectrum (see the Experimental Section).

Reactivity of 2a toward Acids. With the aim of characterizing further the novel complex **2a**, some aspects of its reactivity were investigated, namely, its behavior in the presence of acids and in substitution reactions (see next Section). Notably, despite the presence of two metal−carbon bonds, **2a** is extremely stable in solution and in the solid state, both in air and in the presence of moisture. As a matter of fact, its stability is higher than that of the analogous complex derived from 2,2′-bipyridine, [Pt(bipy-H)(Me)(DMSO)], **3**, which tends to decompose in solution. In the absence of any data regarding decomposition pathways, we can tentatively ascribe the extra stability of pyridyl-quinoline rollover complexes to the peculiar electronic properties of the quinoline ring, able to stabilize additional charges through delocalization in a better way than pyridine.

With the intention to verify the chemical behavior of the Pt−C bonds, we investigated the reactivity of **2a** toward acids. Two acids were tested: HCl and [18-crown-6-H_3O][BF_4], that is, acids having a coordinating and a weakly coordinating counteranion, respectively. As expected, the reaction with aqueous HCl resulted in Pt−CH_3 bond attack with subsequent release of methane, giving the corresponding chloride, [Pt(L-H)(Cl)(DMSO)], **4a**. Only one of the two possible geometric isomers is formed, that is, that with DMSO *trans* to the nitrogen atom, instead of *trans* to the carbon atom, as in **2a**. This is confirmed by the ^1H NMR spectrum of **4a** which shows a $^3J_{Pt-H}$ value, for the coordinated DMSO, strongly enhanced with respect to that found for **2a** (24.0 Hz vs 18.3 Hz), in line with the weaker *trans* influence of N with respect to C. A clear downfield shift is also present for the H_4 proton (δ = 9.02 ppm), attributable to the effect in the space of the DMSO ligand. Also in this case, a 2D COSY spectrum enabled a complete assignment of the ^1H NMR signals. The assignment was supported by a NOESY spectrum, which showed, inter alia, a weak interaction between the DMSO protons, at 3.71 ppm, and the H_4 one, at 9.02 ppm, confirming the proposed geometry.

In contrast, the behavior of **2a** toward [18-crown-6-H_3O][BF_4] is different: the Pt−C bonds remain intact and only protonation of the uncoordinated nitrogen atom occurs, to give the cationic derivative [Pt(L*)(Me)(DMSO)][BF_4], **5a-BF_4**, where L* is the κ^2C,N neutral ligand formed by deprotonation of the C(3)-H atom and protonation of the quinoline nitrogen (Chart 5).

Chart 5

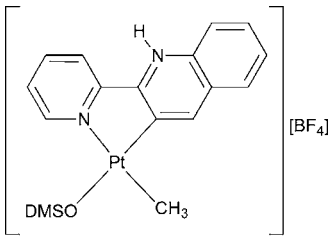

5a-BF_4

The ^1H NMR spectrum of **5a** shows a broad signal at 13.9 ppm, accounting for one hydrogen atom, and ascribable to the N−H proton, which disappears after addition of D_2O. As a further confirmation, the IR spectrum shows bands above 3000 cm^{-1}, due to the N−H stretching.

It is worth to note that the ligands L* and L are isomers. The nature of the former deserves a few comments: it may be described as a mesoionic ligand, but also as an *abnormal remote* pyridylene.[18] The nature of the metal−carbon bond in compounds containing L* ligands has not been fully ascertained, but the distinction between the two representations may be very subtle. Having notable potentialities in catalysis,[52] such uncommon species have received wide attention in recent years. Thus, even if out of the scope of the present contribution, the catalytic activity of **5-BF_4** complexes is reasonably worth of thorough investigation. Worthy of note is also the fact that species **2a** and **5a** constitute an uncommon Brønsted−Lowry acid−base conjugated couple.

The scarce solubility of complex **5a-BF_4** did not allow the acquisition of a ^{13}C NMR spectrum. The analysis of its ^1H NMR spectrum, compared to that of **2a**, showed that the Pt−H coupling constants involving the *trans* Pt−C(sp^2) and Pt−S bonds are greater in the former than in the latter (e.g., $^3J_{Pt-H_4}$ and $^3J_{Pt-CH_3-DMSO}$, see the Experimental Section and reference 19), whereas the contrary is observed for the trans Pt−N and Pt−C(sp^3) bonds (e.g., $^3J_{Pt-H_{6'}}$ and $^2J_{Pt-CH_3}$ in **5a** and **2a**).

dx.doi.org/10.1021/ic400908f | Inorg. Chem. 2013, 52, 7717−7731

Reactivity of 2a and 4a in Substitution Reactions. Starting from **2a** and **4a**, a series of complexes with different electronic and steric properties may be synthesized by substitution of the labile DMSO ligand, as indicated in Chart 6. The substitution is easier in complex **2a** because of the stronger trans influence of carbon compared to nitrogen.

Chart 6

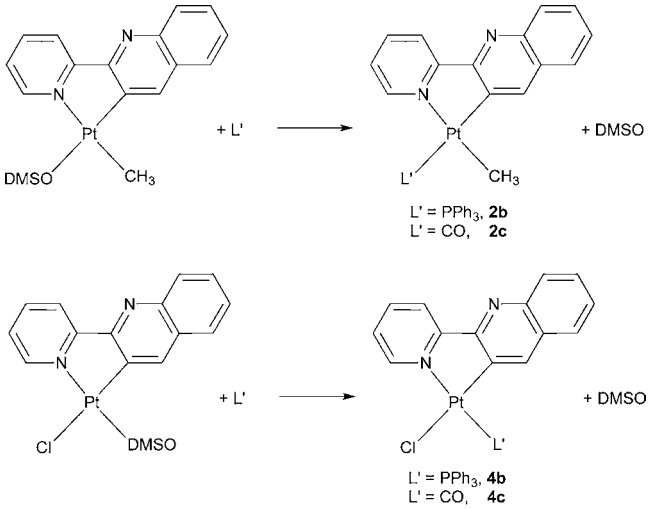

Complexes **2b–c** and **4b–c**, [Pt(L-H)(X)(L′)] (X = Me, L′ = PPh_3, **2b**; X = Me, L′ = CO, **2c**; X = Cl, L′ = PPh_3, **4b**; X = Cl, L′ = CO, **4c**) were isolated in the solid state with good yields and characterized by means of microanalyses, IR and NMR spectroscopy. In particular, the ^{31}P NMR spectra of species **2b** and **4b** clearly indicate a P-*trans*-C geometry for **2b** ($^1J_{Pt-P}$= 2236 Hz) and a P-*trans*-N one for **4b** ($^1J_{Pt-P}$= 4288 Hz), as expected. In the ^1H NMR spectrum of **2b** the platinum-bonded methyl group appears as a doublet with satellites ($^3J_{P-H}$ = 7.5 Hz, $^2J_{Pt-H}$ = 83.1 Hz), providing evidence for a Pt–Me bond in *cis* to a Pt–P one and in *trans* to a Pt–N one. The P-*trans*-C geometry of **2b** was further substantiated by the XRPD structure determination (see next Section).

The IR spectra of the carbonyl species **2c** and **4c** show, as expected, very different CO stretching frequencies: a lower frequency for the electron-rich complex **2c** (ν_{CO} = 2053 cm^{-1}) and a higher frequency (2106 cm^{-1}) for the electron poorer one **4c**. Complex **2c** may have some points of interest having three Pt–carbon bonds, each in a different hybridization state (sp, sp^2, sp^3). Notably, as also confirmed by the XRPD structural analysis (see next Section), the complex contains an uncommon trans C–Pt–C arrangement, usually considered highly unstable because of the high *trans* influence of carbon (*trans-phobia*).[53] Despite this, complex **2c** is highly stable, differently from the analogous rollover complex [Pt(bipy-H)(Me)(CO)],[5] which tends to decompose, and from the cyclometalated complex [Pt(phpy-H)(Me)(CO)] derived from 2-phenyl-pyridine, not isolable in the solid state.[54]

The geometry of complexes **2b** and **2c** in solution was further confirmed by ^1H-NOE 1D spectra, which show NOE contacts between the Pt–Me and the H_4 protons.

As already observed with **2a**, the reaction of the methyl complexes **2b** and **2c** with [18-crown-6-H_3O]$^+$ gave the analogous mesoionic species [Pt(L*)(Me)(PPh_3)]$^+$, **5b**, and [Pt(L*)(Me)(CO)]$^+$, **5c**, (Chart 7) which were isolated in the solid state as tetrafluoborate salts, **5b**-BF_4 and **5c**-BF_4.

As expected, the protonation of the uncoordinated nitrogen atom produces, in the ^1H NMR spectra, a generalized downfield shift of the signals of the aromatic protons. This effect is particularly evident for the H_4 protons (δ 8.64, **2b**; 9.35, **5b**; 8.46, **2c**; 9.17, **5c**). The NH proton gives a broad signal at about 13.8 ppm. A NOE difference spectrum of complex **5b** shows that irradiation at 13.8 ppm promotes enhancement of the doublets at 8.91 and 8.53 ppm, due to the $H_{3'}$ and H_8 protons (Chart 8). In addition, irradiation of the

Chart 8

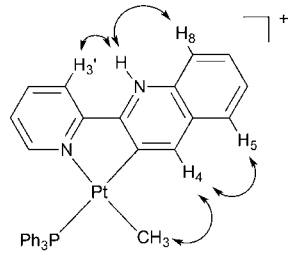

complex **5b**, ^1H NMR NOE contacts

singlet at 9.35 ppm (H_4) shows NOE contacts at 8.05 ppm (d, H_5) and 0.90 ppm (d, Me), confirming the purported geometry of the complex in solution.

The $^1J_{Pt-P}$ value is higher in **5b** (2507 Hz) than in **2b** (2236 Hz), as previously observed for the analogous bipyridine complexes.[5,19]

The CO stretching frequency in **5c**, 2079 cm^{-1}, is higher than in **2c**, 2053 cm^{-1}, as expected because of the minor retrodonating properties of platinum(II) in the cationic complex. These data may be compared to those of the analogous bipyridine-containing couple [Pt(bipy-H)(Me)-(CO)] and [Pt(bipy*)(Me)(CO)]$^+$ (2044 and 2087 cm^{-1}, respectively[55]): the increase of the stretching frequencies, 26

Chart 7

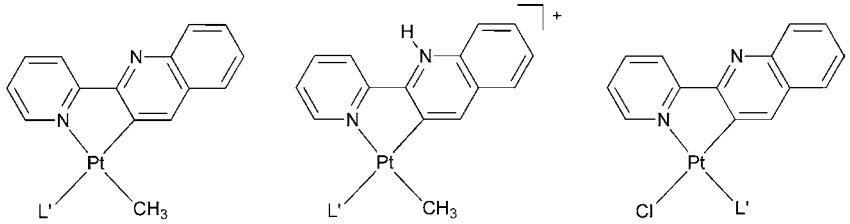

dx.doi.org/10.1021/ic400908f | Inorg. Chem. 2013, 52, 7717–7731

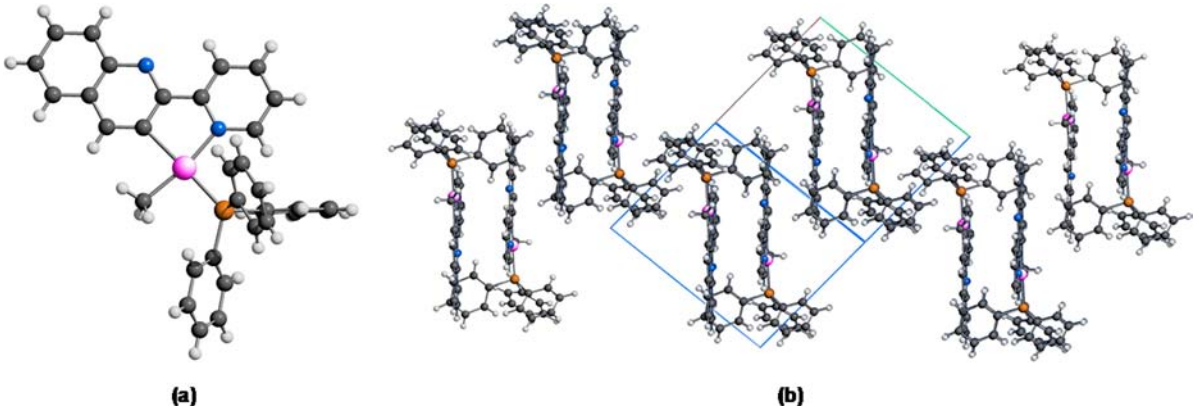

Figure 1. Portion of the crystal structure of species **2b**: (a) the Pt(II) complex; (b) the packing, from which the intermolecular $\pi-\pi$ interactions involving couples of symmetry-related L ligands can be appraised. Carbon, gray; hydrogen, light gray; nitrogen, blue; phosphorus, orange; platinum, fuchsia.

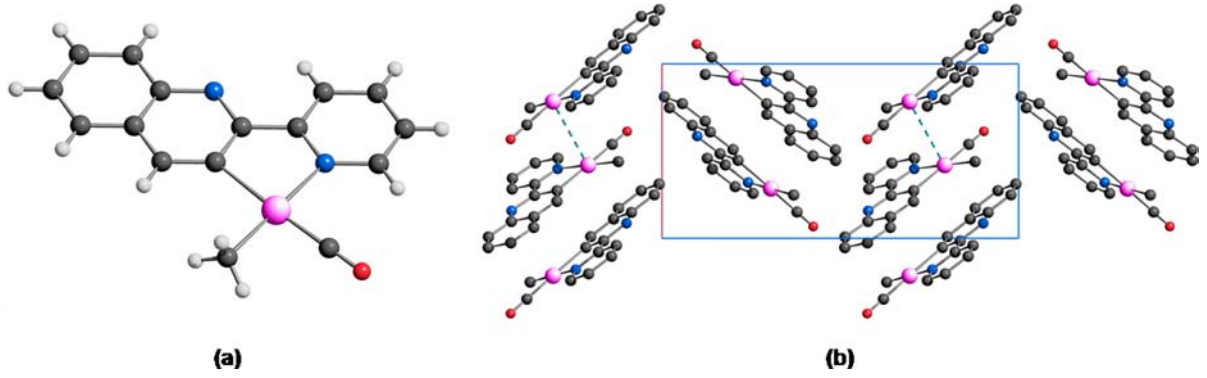

Figure 2. Portion of the crystal structure of species **2c**: (a) one of the two crystallographically independent complexes; (b) the packing, viewed along [001]. Horizontal axis, **a**; vertical axis, **b**. The Pt···Pt non bonding interactions are highlighted with cyan fragmented lines. Hydrogen atoms have been omitted in panel (b) for the sake of clarity. Carbon, gray; hydrogen, light gray; nitrogen, blue; oxygen, red; platinum, fuchsia.

cm^{-1} for L vs 43 cm^{-1} for bipyridine, is very different for the two ligands and may be explained with the greater capacity of L in delocalizing a positive charge, due to the quinoline fragment, so that the Pt−C−O bonds are less affected by the additional charge than in the bipyridine-based complexes, for which the protonation directly results in a stronger change in the C−O bond order.

Reactivity of 4b. Protonation of complex **4b** with [18-crown-6·H_3O]$^+$ allows the isolation of the corresponding mesoionic species [Pt(L*)(Cl)(PPh_3)][BF_4], **6-BF$_4$**. A broad signal at 13.9 ppm in the ^{1}H NMR spectrum provides evidence of the protonation of the nitrogen atom. The analysis of the ^{1}H NMR spectra of **4b** and **6** shows that all the signals of the aromatic protons are deshielded after protonation, as expected. In contrast to the **2b**−**5b** couple, in the present case the ^{195}Pt−^{31}P coupling constant decreases after protonation (4143 Hz in **6** vs 4288 Hz in **4b**), indicating that *cis* and *trans* influences have a predominant effect on the coupling constant in these species. In particular, coupling constant values for bonds in *trans* to C_3 increase after protonation, whereas those for bonds in *cis* to C_3 follow an opposite trend. Unfortunately, it is not straightforward to establish whether these data really indicate strengthening and weakening of the corresponding Pt−ligand bonds.

X-ray Powder Diffraction Structural Analysis of 2b, 2c, and 5c-BF$_4$. The crystal and molecular structures of species **2b**, **2c**, and **5c-BF$_4$** were retrieved from state-of-the-art X-ray powder diffraction (XRPD) methods. Relying on the extended use of rigid bodies, structure determinations from XRPD do not afford, for the geometrical parameters, the accuracy typical of single-crystal X-ray diffraction analyses. Nevertheless, the inter- and supra-molecular features can be confidently derived. This relevant, otherwise inaccessible, piece of information will thus be discussed in the following for **2b**, **2c**, and **5c-BF$_4$**.

As detailed in the Experimental Section, the rollover nature of the Pt(II) complex was ascertained in all the cases by the thorough NMR characterization: a rigid body model comprising a *C,N*-chelating ligand was consequently adopted. Nonetheless, the possibility of having the methyl group *trans* to the Pt-coordinated carbon atom was investigated during the structure solution stage. The structural models with the lowest figures of merit always possessed the *trans* Me−Pt−N geometry suggested by NMR. These models were thus selected for the final structure refinements.

Species **2b** crystallizes in the triclinic space group $P\bar{1}$. Its asymmetric unit comprises one [Pt(L-H)(Me)(PPh_3)] complex (Figure 1a), lying on a general position. The steric hindrance is responsible for the actual orientation of the PPh_3 moiety, no phenyl ring being obviously coplanar with the L ligand. The reciprocal disposition of the complexes is dictated by the formation of intermolecular $\pi-\pi$ interactions between couples of parallel L ligands, lying approximately on the (11−2) plane, and facing each other at about 3.4 Å (Figure 1b). The two $\pi-\pi$ interacting complexes are mutually related by a

dx.doi.org/10.1021/ic400908f | Inorg. Chem. 2013, 52, 7717−7731

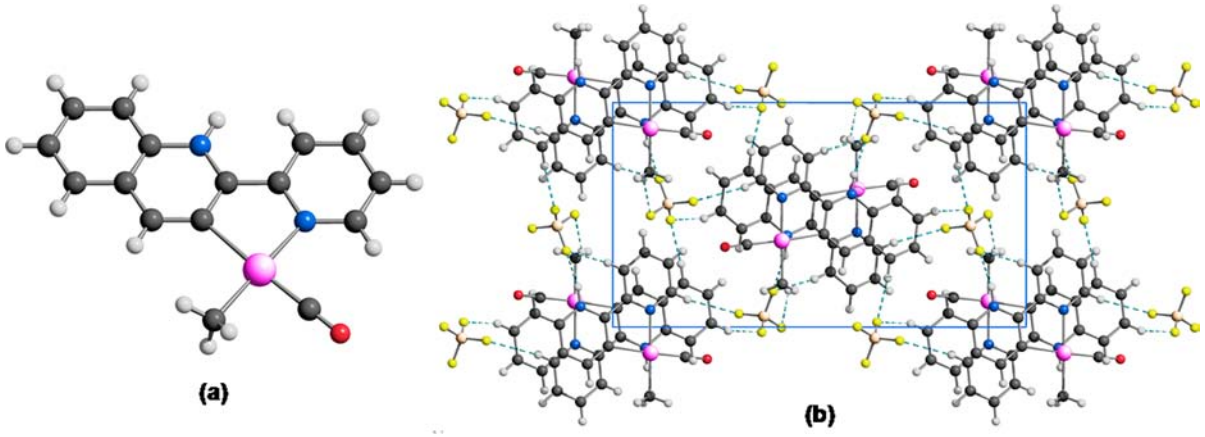

Figure 3. Portion of the crystal structure of species **5c-BF$_4$**: (a) the cationic complex; (b) the packing, viewed along **c**. Horizontal axis, **a**; vertical axis, **b**. The weak C−H···F interactions involving neighboring BF_4^- anions and cationic complexes are highlighted in panel (b) with cyan fragmented lines. Carbon, gray; hydrogen, light gray; boron, light orange; fluorine, yellow; nitrogen, blue; oxygen, red; platinum, fuchsia.

crystallographic inversion center; thus, no Pt···Pt contacts can be appraised together with the $\pi-\pi$ ones.

Species **2c** crystallizes in the monoclinic space group $P2_1$. The asymmetric unit contains two, crystallographically independent, [Pt(L-H)(Me)(CO)] complexes (Figure 2a). The two independent complexes lie approximately on the (210) plane (and on the symmetry related one (2−10)), and form piles of staggered moieties along [210]. Along the piles, Pt···Pt contacts of about 3.4 Å can be envisaged between couples of consecutive complexes (Figure 2b). Visualized along the crystallographic axis **c**, the adjacent stacks describe a herringbone motif.

Species **5c-BF$_4$** crystallizes in the monoclinic space group $P2_1/n$. Its asymmetric unit contains one cationic $[Pt(L^*)(Me)(CO)]^+$ complex (Figure 3a) and one BF_4^- anion, both lying on general positions. The cationic complexes lie approximately parallel to the (−302) plane and stack, staggered, along **c** with a pace of $c/2$ (Figure 3b), so that no intermolecular $\pi-\pi$ and Pt···Pt interactions are at work. The anions are located between the stacks (Figure 3b), their actual orientation being imposed by the formation of weak C−H···F interactions involving three nearby complexes (C···F 2.74−3.14 Å).

DFT-Calculated Molecular Structures of 2a−c and 5a−c. In square planar complexes having a chelating ligand that blocks two positions, as in **2a−c** and **5a−c**, two isomers are possible, namely, one with the methyl residue *trans* to the nitrogen atom, and the other where the methyl group is *trans* to the metalated carbon atom (Scheme 3). In the next part of the discussion, we will call "experimental" the former, retrieved from NMR spectroscopy, and "inverted" the latter; moreover a prime will be used to distinguish the two species.

Complexes $[Pt(L\text{-}H)(CH_3)(DMSO)]$, $[Pt(L\text{-}H)(CH_3)(PPh_3)]$, $[Pt(L\text{-}H)(CH_3)(CO)]$, $[Pt(L\text{-}H)(CH_3)(DMSO)]^+$, $[Pt(L^*)(CH_3)(PPh_3)]^+$, $[Pt(L^*)(CH_3)(CO)]^+$ (**2a−c** and **5a−c**), and their corresponding "inverted" isomers (**2a′-c′** and **5a′-c′**, Scheme 3) were optimized at the PBE0/def2-SVP level of theory. In each case the isomer deduced from the NMR data is the one that displays a lower energy; the calculated relative enthalpy and Gibbs free energy differences (298.15 K and 1 atm) are collected in Table 1 where the isomer having the lowest energy has been taken as reference. As expected, more than 90% of the "stabilization energy" comes from an enthalpic factor because the entropic contribution is very similar in both isomers and, consequently, its role in stabilizing the experimental isomer is less important. This observation fits well in the framework of *trans*-phobia[53] and antisymbiosis effect.[56]

As described above, upon reaction with [18-crown-6·H_3O]-[BF_4], complexes **2a−c** yield the cationic N-protonated analogues **5a−c**. As made evident from the calculations, both protonation and change in the charge of the complex cause only slight modifications in bond distances and angles (see Table 2 and Table 3). Changes in bond distances involving platinum can be explained in terms of push−pull interactions between ligands *trans* to each other, that is, when a bond elongates, that in *trans* shortens. In detail, the highest variations, in absolute value, are evident for Pt−$N_{1'}$, Pt−CH_3, and Pt−L

Scheme 3. Experimental (2a−c) and "Inverted" (2a′-c′) Isomers Studied[a]

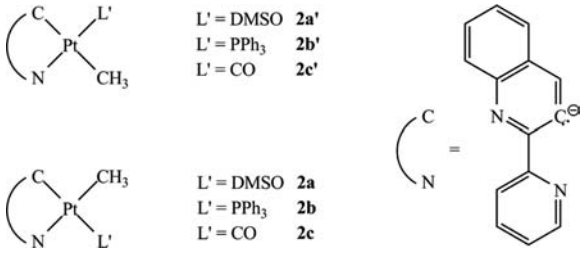

[a]The energies were evaluated also for the corresponding cationic species **5a−c** and **5a′−c′**.

Table 1. DFT-Calculated Relative Enthalpy (ΔH) and Gibbs Free Energy (ΔG)[a] Differences between Experimental and "Inverted" Isomers, Taking the Former As Zero[b]

complex	ΔG	ΔH
$[Pt(L\text{-}H)(CH_3)(DMSO)]$, **2a**	48.8	46.8
$[Pt(L^*)(CH_3)(DMSO)]^+$, **5a**	39.7	37.7
$[Pt(L\text{-}H)(CH_3)(CO)]$, **2c**	14.4	12.8
$[Pt(L^*)(CH_3)(CO)]^+$, **5c**	17.7	16.2
$[Pt(L\text{-}H)(CH_3)(PPh_3)]$, **2b**	23.1	20.1
$[Pt(L^*)(CH_3)(PPh_3)]^+$, **5b**	17.0	17.7

[a]Both ZPE corrected, T = 298.15 K, P = 101325 Pa. [b]All the values are expressed in kJ mol^{-1}.

dx.doi.org/10.1021/ic400908f | Inorg. Chem. 2013, 52, 7717−7731

Table 2. DFT-Calculated Bond Distances (pm) and Angles (deg) around the Metal Center for Complexes 2a−c and the Corresponding Protonated Species 5a−c[a]

	DMSO		CO		PPh_3	
	2a	5a	2c	5c	2b	5b
Pt−L′	233.0	233.1	190.3	190.9	235.0	235.8
Pt−CH_3	205.5	204.6	205.9	205.3	205.8	204.9
Pt−$N_{1'}$	215.6	217.3	216.5	217.9	217.5	219.1
Pt−C_3	201.5	201.4	205.3	205.3	203.8	203.7
$N_{1'}$−Pt−C_3	80.3	79.5	79.7	79.0	79.6	78.8
C_3−Pt−CH_3	91.0	91.5	90.8	91.4	89.9	90.5
CH_3−Pt−L′	90.4	90.4	89.7	88.7	86.0	85.7
L′−Pt−$N_{1'}$	98.2	98.5	99.8	100.9	104.6	105.0
$N_{1'}$−Pt−CH_3	171.3	171.1	170.5	170.4	169.3	169.2
C_3−Pt−L′	178.5	178.0	179.5	179.9	175.6	176.0

[a]For the atom labels, consult Scheme 2.

Table 3. DFT-Calculated Bond Distances (pm) of the Cyclometalated Ligand in Complexes 2a−c and 5a−c[a]

	DMSO		CO		PPh_3	
L′	2a	5a	2c	5c	2b	5b
$N_{1'}$−$C_{2'}$	134.9	133.5	134.8	135.2	135.0	135.4
$C_{2'}$−$C_{3'}$	139.5	139.6	139.7	139.5	139.7	139.6
$C_{3'}$−$C_{4'}$	138.8	138.8	138.7	139.2	138.7	139.2
$C_{4'}$−$C_{5'}$	139.4	139.3	139.6	139.0	139.4	138.9
$C_{5'}$−$C_{6'}$	139.1	139.4	138.8	139.3	139.0	139.4
$C_{6'}$−$N_{1'}$	134.0	135.3	133.8	133.3	133.8	133.4
$C_{2'}$−C_2	147.3	146.7	147.6	147.2	147.3	146.8
C_2−N_1	131.4	141.6	131.5	134.2	131.6	134.3
C_2−C_3	143.5	139.1	143.5	141.3	143.4	141.4
C_3−C_4	138.0	141.4	138.0	139.0	138.1	139.3
C_4−C_5	141.8	142.1	141.8	141.4	141.8	141.4
C_5−C_6	141.8	136.5	141.8	141.9	141.9	141.9
C_6−C_7	137.6	134.1	137.6	137.5	137.6	137.5
C_7−C_8	141.6	141.9	141.6	141.5	141.6	141.5
C_8−C_9	137.5	137.5	137.5	137.8	137.5	137.7
C_9−C_{10}	142.0	141.5	142.0	140.8	142.0	140.8
C_{10}-N_1	135.1	137.8	135.1	136.6	135.0	136.4
C_{10}−C_5	142.9	140.8	143.0	142.2	142.9	142.1

[a]For the atom labels, consult Scheme 2.

bonds (ca. 1 pm). Quite surprisingly, the Pt−$C_{3'}$ bond length is almost unchanged, showing a 0.1 pm difference which is too small to be considered significant.

The angles insisting on the metal center do not show dramatic changes in their absolute value, but it can be noted that corresponding angles have the same trend, that is, $N_{1'}$−Pt−C_3 and L−Pt−CH_3 close, while the other two become wider (Table 2). Finally, the planarity of the molecule is not affected by the protonation of the noncoordinating quinolinic nitrogen.

The effect of protonation on the cyclometalated ligand was also investigated (Table 3). As is expected, the changes in the molecular structure are more pronounced in the surroundings of the protonation site and, particularly, in the N_1−C_2, C_2−C_3, N_1−C_{10} and C_9−C_{10} bond lengths, with elongations of about 3.0, 2.0, 1.4, and 1.2 pm, respectively. Interestingly, a kind of "contraction" of the metallacycle bonds is evident on the quinolinic moiety, that is, $C_{2'}$−C_2, C_2−C_3, and, to a lesser extent, C_3−Pt. This is in line with the fact that the electron density is somewhat pulled toward the protonated nitrogen, which is more electron-deficient than in the neutral complex.

The bonds in the pyridinic ring rearrange without significant or unexpected changes: all the differences are below 1 pm; in detail, those bonds closer to the quinolinic system (i.e., $N_{1'}$-$C_{2'}$ and $C_{2'}$-$C_{3'}$) shorten, while the others are alternately shorter or longer.

The trend of the unscaled stretching frequencies of the CO bond in complexes **2c** and **5c**, recorded in Nujol, is correctly reproduced by the harmonic analysis: 2053 vs 2183 cm^{-1} for the neutral species, and 2079 vs 2225 cm^{-1} for the protonated one (the first wavenumber value is the experimental one).

Finally, evaluation of the DFT-calculated proton affinity and gas phase basicity of the species **2a−c** (Table 4) and comparison with the corresponding bipyridine analogues, respectively [Pt(bipy-H)(CH_3)(DMSO)], [Pt(bipy-H)(CH_3)(PPh_3)], and [Pt(bipy-H)(CH_3)(CO)], permits to note the following: (a) both with L and bipy the easiness of protonation depends on the neutral ligand coordinated *trans* to the metalated carbon atom and increases in the order PPh_3 > DMSO > CO; (b) complexes with cyclometalated bipy always show lower values than the corresponding with L. These observations are in good agreement and show a good correlation with the well-known donor properties of the neutral ligands involved in this work; moreover it seems that the basicity order expected for pyridine and quinoline is respected.

Table 4. DFT-Calculated Proton Affinity (ΔH) and Gas Phase Basicity (ΔG)[a] for Complexes 2a−c and the Corresponding Bipyridine Analogues[b]

complex	ΔG	ΔH
[Pt(L-H)(CH_3)(DMSO)], **2a**	1007.5	1005.3
[Pt(L-H)(CH_3)(PPh_3)], **2b**	1027.4	1026.8
[Pt(L-H)(CH_3)(CO)], **2c**	980.3	978.6
[Pt(bipy-H)(CH_3)(DMSO)]	995.1	993.1
[Pt(bipy-H)(CH_3)(PPh_3)]	1018.6	1016.1
[Pt(bipy-H)(CH_3)(CO)]	964.8	963.2

[a]Both ZPE-corrected. [b]All the values are expressed in kJ mol^{-1}.

Electronic Spectroscopy and Electrochemical Behavior. Platinum derivatives **2a−c** and **5a−c** were characterized by UV−vis spectroscopy in CH_2Cl_2. By comparison with the free ligand, the higher energy bands are attributable to ligand centered $\pi-\pi^*$ transitions and the lower ones are tentatively assigned to metal-to-ligand charge transfer transitions (380−430 nm).[57] N-protonated cationic derivatives show MLCT absorptions at higher wavelengths than the corresponding neutral species, suggesting a more effective extension of the charge delocalization on the complex. It seems reasonable to ascribe this red-shift of the MLCT band to the effects that the protonation has on the electron density, as highlighted also by the DFT calculations (see Table 5). The same effect can be observed comparing complexes **2a** and **3**, which differ only for the cyclometalated ligand (L and bipy, respectively) thus we are prone to think that the higher extent in the electronic delocalization originating from the quinoline system instead of a pure pyridine ring is the reason of the observed red-shift. The analysis of the UV−vis bands position permits also to roughly estimate the σ-donor effect of the cyclometalated ligand.[57] Complexes **2a** and **3** show λ_{max} respectively at 403 and 380 nm suggesting that bipy-H has a stronger σ donating effect

dx.doi.org/10.1021/ic400908f | Inorg. Chem. 2013, 52, 7717−7731

Table 5. Electrochemical, Optical, and Computational Data

compound	λ(nm)[a]	Eg,opt (eV)[b]	Eg,theor (eV)[c]	E_{ox} (V)[d]	E_{red}(V)[d]	$HOMO_{exp}$ (eV)	$LUMO_{exp}$ (eV)	$HOMO_{theor}$ (eV)[c]	$LUMO_{theor}$ (eV)[c]
[Pt(bipy-H)(DMSO)(Me)] (**3**)	276, 307, 380	2.99	4.71	0.72		−5.13[e]	−2.14[f]	−6.28	−1.57
[Pt(bipy*)(DMSO)(Me)]	255, 314, 364	2.95	3.75		−0.58	−7.42[f]	−4.47	−9.73	−5.98
[Pt(L-H)(DMSO)(Me)] (**2a**)	306, 366, 403	2.94	4.37	0.64		−5.04[e]	−2.89[f]	−6.15	−1.78
[Pt(L*)(DMSO)(Me)]$^+$ (**5a**)	325, 460	2.18	3.43		−0.85	−6.74[f]	−4.56[e]	−9.54	−6.11
[Pt(L-H)(PPh3)(Me)] (**2b**)	262,302, 381	2.88	4.23	1.35		−5.70[e]	−2.71[f]	−5.89	−1.66
[Pt(L*)(PPh_3)(Me)]$^+$ (**5b**)	264, 329, 429	2.46	3.06		−0.50	−7.00[f]	−4.54[e]	−8.87	−5.81
[Pt(L-H)(CO)(Me)] (**2c**)	256, 289	3.59	4.36	1.21		−5.61[e]	−2.02[f]	−6.48	−2.12
[Pt(L*)(CO)(Me)]$^+$ (**5c**)	275, 284, 350	2.96	3.71		−0.44	−7.69[f]	−4.73[e]	−10.17	−6.46
L	253, 320, 335	3.62	4.95 (cis)	1.58		−5.59[e]	−1.97[f]	−6.66 (cis)	−1.71 (cis)
			4.83 (trans)					−6.64 (trans)	−1.81 (trans)

[a]Measured in CH_2Cl_2 solution. Concentration for UV−vis measurements was about 2×10^{-5} M. [b]The energy-gap (Eg,opt) value was determined from the λ_{onset} in the UV−vis spectrum. [c]Theoretical values obtained from DFT calculations at PBE0/def2-SVP level. [d]Potential values reported vs Ag/AgCl in CH_2Cl_2-$TEAPF_6$ 0.1 M solvent system. Concentration 2×10^{-3} M. [e]Calculated from the anodic (HOMO) or cathodic (LUMO) onset potential value. [f]The LUMO energy value was calculated from the equation LUMO(eV) = HOMO + Eg,opt, and the HOMO value from HOMO(eV) = LUMO − Eg,opt. (reference 59).

than L-H; the same trend is visible in the corresponding N-protonated species **5a**, [Pt(L*)(Me)(DMSO)]$^+$, and [Pt(bipy*)(Me)(DMSO)]$^+$ (460 vs 364 nm).

The analysis of the energy-gap (Eg) values derived from the UV−vis spectra evidence, as predictable, a lower Eg value for the cationic complexes (**5a−c**) than for the corresponding neutral ones (**2a−c**). Eg values obtained from UV−vis spectra were compared with estimated data by DFT method (see Table 5), confirming a decrease in Eg values going from neutral to cationic species. Differences in experimental with respect to calculated Eg data is between 18 and 36%: although such values seem quite high, they are in line with those reported for some Pt(II) derivatives with phenylpyridine and benzoquinoline ligands.[58] We reasonably impute the difference to the functional/basis set used in the computations and the absence of the solvent which can play a not negligible role.

Finally, the analysis of the molecular orbitals suggests that the higher Eg displayed by the bipy-H complexes is due to a concurrent stabilization of the highest occupied molecular orbital (HOMO) and destabilization of the lowest unoccupied molecular orbital (LUMO).

The electrochemical behavior of the neutral (**2a−c**) and of the corresponding cationic (**5a−c**) species was investigated in the CH_2Cl_2-$TEAPF_6$ 0.1 M solvent system by cyclic voltammetry.

Neutral complexes show an anodic irreversible process between 0.6 and 1.4 V, while the oxidation of the free ligand occurs at about 1.6 V (Table 5). DFT calculations indicate that in the free ligand the HOMO is located on the whole of the molecule, while in the complexes it encompasses the quinoline fragment, the metal center, and, especially in the case of **2c**, even the L′ ligand. Theoretical data support the hypothesis that the anodic processes involve primarily the pyridylquinoline ligand (L), and to a minor extent the Pt(II) center and, eventually, the L′ ligand. Moreover, DFT data show a dipole moment oriented toward the L′ ligand in **2a** and **2b**, and toward the pyridine ring in **2c**. The comparison between the direction of the dipole moment, together with the fact that the oxidation process is mainly located on L, might explain the higher oxidation potential of the PPh_3 derivative (**2b**) compared to the CO one (**2c**): as a matter of fact, in **2b** the electron density on the quinoline ring is lower than in **2c**, thus the oxidation process in the latter is easier than in **2b**. In the case of the dimethylsulfoxide (DMSO) derivative (**2a**), the known lability of the Pt−DMSO bond makes it difficult to compare its electrochemical response with that of the analogues **2b** and **2c**.

The cathodic portion of the voltammograms does not evidence the appearance of reductive processes in the potential range exploited. With regards to the LUMO values, the DFT calculations seem to confirm that the associated cathodic process would be at very negative onset potential values, reasonably not detectable in the CH_2Cl_2-$TEAPF_6$ solvent system.

As for the cationic species (**5a−c**), no oxidative process is evidenced in the potential range exploited. Evaluation of the HOMO energy values by DFT calculations suggest that the anodic response due to the cationic species, mainly located on the metal center, would be at potential values higher than the anodic limit of the CH_2Cl_2-$TEAPF_6$ 0.1 M solvent system. Conversely, the cathodic behavior shows a reduction process (Table 5) attributable to the reduction of the protonated portion. The DFT data indicate that the LUMO is always located on the pyridylquinoline ligand, and the dipole moment is always oriented toward the cyclometalated ligand, L, accounting for the relatively small difference between the reduction potential values of **5b** and **5c**.

Accordance between experimental and theoretical data is in the range of analogous comparisons reported in literature.[58]

Retro-Rollover Process Involving 5b. The mesoionic species **5a** and **5c** are rather stable in solution and do not decompose in the presence of moisture or oxygen. However, the NMR spectrum of complex **5b**, acquired in $CDCl_3$, undergoes a slow change; as a matter of fact, both ^1H and ^{31}P NMR show the conversion of **5b** into two new species (**7**), formed in a 1.3:1 molar ratio. The new complexes appear to be very similar, each having, inter alia, one methyl group and one phosphorus atom bound to platinum, with similar $^{195}Pt-^1H$ and $^{195}Pt-^{31}P$ coupling constant values (see the Experimental Section), suggesting P−Pt−N and Me−Pt−N *trans* coordination for both complexes.

dx.doi.org/10.1021/ic400908f | Inorg. Chem. 2013, 52, 7717−7731

Scheme 4. Retro-Rollover Process

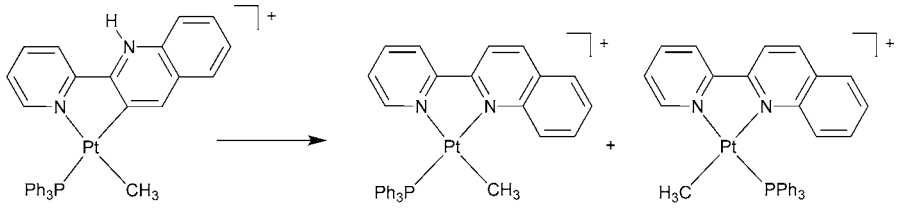

These similarities suggest that the two species are closely related, being the two geometric isomers of $[Pt(L)(Me)(PPh_3)]^+$ (Scheme 4), originated through a "retro-rollover" process, as recently reported by some of us for the analogous bipyridine complexes.[19] In the starting complex **5b**, the C_3 atom is metalated, so the appearance of the signals due to the H_3 protons in the spectra of both species strongly corroborates our assumption. Furthermore, in the aromatic region, a signal with satellites is clearly visible which is typical of an H_6 proton *trans* to phosphorus,[19] due to a N−Pt−P *trans* arrangement, whereas in the other isomer the signal due to H_6 is strongly upfield shifted (δ = 7.65 ppm) by the shielding cones of the phosphine aromatic rings. In the light of this, the two species may be indicated as **7t** (phosphorus *trans* to quinoline) and **7c** (phosphorus *cis* to quinoline). As expected, complex **7t**, having the bulky PPh_3 far from the quinoline moiety, is the main species. In line with this assignment, NOESY-1D spectra showed contacts between the methyl group at 0.72 ppm (Pt−Me in **7t**) and a doublet at 8.40 ppm belonging to the adjacent H_8 proton. For the other Pt−Me hydrogens, that is, those of the **7c** isomer, a clear contact with the $H_{6'}$ proton, at 8.94 ppm, is observed. A H−H COSY spectrum further helped in the assignments; in particular, two AB systems, due to the H_3 and H_4 protons, are clearly visible in the spectra.

The retro-rollover isomerization reaction likely proceeds through protonation of platinum(II) following an oxidative-addition/reductive-elimination reaction pathway. The reductive elimination step is followed by rotation around the C−C bond between the aromatic rings and by chelation. A second possible reaction pathway, that is, a concerted mechanism involving electrophilic attack of the platinum−carbon bond, cannot be completely ruled out, but in the case of electron-rich platinum(II) organometallic complexes it is unlikely.[60] According to the first mechanism, electron-richer complexes react faster than electron-poorer species.

The retro-rollover reaction rate is solvent-dependent: the process is slower in $CDCl_3$ (approximately 30% conversion in a 10^{-2} M solution after 2 days) and faster in CD_2Cl_2 (100% conversion after 2 days). Addition of excess crown ether acid does not affect the reaction rate, probably because protonation of Pt does not occur on the cationic species **5** but on the neutral complexes **2**, originated from **5** by deprotonation. Dilution of the solution results in a slower reaction rate, so it is likely that the process is not intramolecular, but may involve water. Saturation with H_2O almost inhibits the reaction, but this may be due to the presence of a water phase, so that H_3O^+ is partially removed from the chloroform solution.

The analogous conversion of the bipyridine rollover[19] complex $[Pt(bipy^*)(Me)(PPh_3)]^+$ is significantly slower, reaching completion in CD_2Cl_2 only after 30 days. In this case, the reaction rate was shown to be strongly dependent on the electron density on the metal center. In particular, studying the effect of the phosphane properties in the rollover complexes $[Pt(bipy^*)(Me)(PR_3)]^+$, it emerged that better donors (e.g., P(p-tolyl)$_3$ vs PPh_3) highly accelerate the process. Moreover, we have found that also the nature of the cyclometalated ligand strongly affects the rate of reaction. The condensed aromatic ring on the cyclometalated pyridine is likely to strongly favor the retro-rollover process. However, although electronic effects seem to be dominant, also steric ones may play a non negligible role. In particular, repulsion between the N−H and the H_8 protons (in mutual peri position, Chart 9), added to the N−H vs $H_{3'}$ repulsion, may also influence the process.

Chart 9

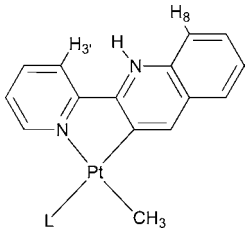

Protonolysis of M−CH_3 bonds is considered as the microscopic reverse reaction of the activation of alkane C−H bonds, and hence it has been the subject of extensive mechanistic investigations.[31] To the best of our knowledge, all the cases reported in the literature refer to Pt−C(alkyl) bond cleavage, rather than to Pt−C(aryl) rupture. Thus, the retro-rollover process is the first case of preferred Pt−C(sp^2) bond protonolysis in place of Pt−C(sp^3). This occurrence may have future potential applications in catalysis, in processes where a heterocyclic bidentate donor may act as a hydrogen reservoir/acceptor.

Complexes **7** are not static in solution: a 1D-EXSY experiment in CD_2Cl_2 showed that irradiation of the methyl signal at 0.92 ppm (**7t**, main species), results in magnetization transfer to the other methyl group at 0.67 ppm, demonstrating a dynamic process in solution which rapidly interconverts the two isomers on the NMR time scale (Chart 10).

Chart 10

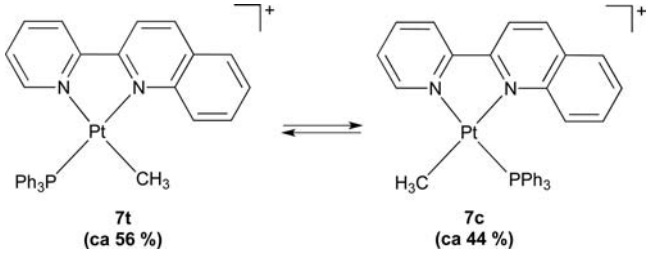

dx.doi.org/10.1021/ic400908f | Inorg. Chem. 2013, 52, 7717−7731

An analogous behavior was observed by Romeo and coworkers in the case of the symmetric chelating ligand 2,9-dimethyl-1,10-phenanthroline (N,N) in a series of cationic $[Pt(N,N)(Me)(PR_3)]^+$ complexes.[61] By contrast, analogous complexes of the less-hindered ligands 1,10-phenanthroline and 2,2′-bipyridine, appear static in solution on the NMR time scale. The severe distortion of the square planar geometry around the platinum center, due to the methyl groups on the bidentate ligand 2,9-dimethyl-1,10-phenanthroline, was reported to be responsible for the fluxionality of the complexes. Detailed kinetic studies showed that the mechanism of the process may switch from associative to dissociative pathways according to several factors, such as solvent or counterion properties, the presence of external nucleophiles, the electronic and steric properties of the phosphane ligand, and so forth. In addition to the flipping of the bidentate N,N ligand, also rotation of the phosphane occurs. Indeed, it was shown that tuning the bulkiness of the PR_3 ligand, the two motions display identical rates. Because of this synchronized fluxional motion, these complexes act as a molecular gear.[61d,e]

To the best of our knowledge, complexes **7c** and **7t** are the first platinum(II) species with nonsymmetric N,N chelating ligands which show a dynamic flipping of the chelated ligand. The possibility to design molecular gears whose dynamics can be controlled by the stereoelectronic properties of the ligands is of outstanding interest. Studies are in progress to evaluate, also in the present case, the possible behavior as a molecular gear with different phosphane ligands.

Finally, it is worth noting that $[Pt(N,N)(Me)(\text{neutral ligand})]^+$ cationic complexes are also of interest in the C−H bond activation of alkanes,[62] even if their synthesis is usually not so straightforward, involving the use of silver salts and several steps. On the contrary, our methodology opens a new and simpler way to obtain this class of complexes, at least when the rollover reaction is accessible.

CONCLUSIONS

The 2-pyridyl-quinoline ligand, despite of its similarity to 2,2′-bipyridine, has a more complex behavior because of differences both in the electronic and in the steric properties. Because of its specific features, both rollover and retro-rollover processes are highly favored and accelerated.

Protonation of the uncoordinated nitrogen atom in the rollover species **2a−c** allowed the synthesis of the series of uncommon species **5a−c**. Complexes **2** and **5** are unusual Brønsted−Lowry acid−base couples, which may be considered from several points of view. Complexes **5a−c** may be described as mesoionic species, abnormal-remote carbenes, or pyridylenes, and the ligand L* is an isomer, or a tautomer, of the free ligand L. Furthermore, the L/L* couple is an example of a "*Ligand with multiple personalities*",[63] a class of ligands with additional N−H bonds which is receiving growing interest. These species have been reported to respond to variations in the solution environment, such as pH changes, modifying the properties of the transition metal center and raising interesting perspectives in C−H bond activation[64] and in the design of molecular devices.[65]

The nature of the mesoionic species **5a−c** and **6** has not been fully investigated. An interesting feature is the trend of the NMR data, which show that in this family of complexes the coupling constant values around the platinum center are governed by position more than by charge: the coupling constant values in *trans* to C(3) increase after protonation, whereas those in *cis* position decrease. This is a clear example of *trans* vs *cis* influence.

The retro-rollover process, which is particularly fast with the ligand L, may be of future interest because of its potential applications in catalytic cycles, for example, in the dehydrogenation of alcohols,[1a] with L serving as hydrogen atom reservoir, or in functionalization reactions.[13]

It is also a unique example of Pt−C(sp^3) vs Pt−C(sp^2) protonolysis, an interesting result in view of the close relationship between M−C protonolysis reactions and metal-mediated C−H bond activation, that is, the reverse process. Notably, for the first time a retro-rollover process is observed for a "non-symmetric" rollover complex. Furthermore, the final species, the cationic adduct $[Pt(L)(Me)(PPh_3)]^+$, has been demonstrated to be fluxional in solution.

Finally, for the first time, the X-ray crystal structure of a protonated rollover species, **5c-BF$_4$**, has been determined and reported.

ASSOCIATED CONTENT

Supporting Information

Final Rietveld refinement plots for species **2b**, **2c**, and **5c-BF$_4$**. DFT calculated equilibrium geometries, energy values, dipole moments, molecular orbitals and TD-DFT calculated transitions. This material is available free of charge via the Internet at http://pubs.acs.org.

AUTHOR INFORMATION

Corresponding Author

*E-mail: zucca@uniss.it.

Notes

The authors declare no competing financial interest.

ACKNOWLEDGMENTS

Financial support from Università di Sassari and Ministero dell'Università e della Ricerca Scientifica is gratefully acknowledged. We thank Johnson Matthey for a generous loan of platinum salts, and Norberto Masciocchi for definitely fruitful discussions. L.M. gratefully acknowledges a PhD fund, financed by POR/FSE 2007-2013, from Regione Autonoma della Sardegna and the resources given by the Cybersar Project managed by the "Consorzio COSMOLAB".

REFERENCES

(1) (a) For example, see Albrecht, M. *Chem. Rev.* **2010**, *110* (2), 576−623. (b) Omae, I. *Coord. Chem. Rev.* **2004**, *248* (11−12), 995−1023.

(2) Butschke, B.; Schwarz, H. *Chem. Sci.* **2012**, *3*, 308−326.

(3) (a) Skapski, A. C.; Sutcliffe, V. F.; Young, G. B. *J. Chem. Soc., Chem. Commun.* **1985**, 609−611. (b) Minghetti, G.; Stoccoro, S.; Cinellu, M. A.; Soro, B.; Zucca, A. *Organometallics* **2003**, *22* (23), 4770−4777.

(4) Butschke, B.; Schwarz, H. *Organometallics* **2010**, *29* (22), 6002−6011.

(5) Zucca, A.; Petretto, G. L.; Stoccoro, S.; Cinellu, M. A.; Manassero, M.; Manassero, C.; Minghetti, G. *Organometallics* **2009**, *28* (7), 2150−2159.

(6) Doppiu, A.; Minghetti, G.; Cinellu, M. A.; Stoccoro, S.; Zucca, A.; Manassero, M. *Organometallics* **2001**, *20* (6), 1148−1152.

(7) (a) Giordano, T. J.; Rasmussen, P. G. *Inorg. Chem.* **1975**, *14* (7), 1628−1634. (b) Nonoyama, M. *Bull. Chem. Soc. Jpn.* **1979**, *52*, 3749−3750. (c) Nonoyama, M.; Kajita, S. *Transition Met. Chem.* **1981**, *6* (3), 163−165. (d) Chassot, L.; Von Zelewsky, A. *Inorg. Chem.* **1987**, *26* (17), 2814−2818. (e) Chang, S. C.; Hauge, R. H.; Billups, W. E.;

Margrave, J. L.; Kafafi, Z. H. *Inorg. Chem.* **1988**, *27* (1), 205−206. (f) Gianini, M.; Von Zelewsky, A.; Stoeckli-Evans, H. *Inorg. Chem.* **1997**, *36* (26), 6094−6098. (g) Fuchita, Y.; Ieda, H.; Wada, S.; Kameda, S.; Mikuriya, M. *J. Chem. Soc., Dalton Trans.* **1999**, 4431−4435. (h) Lee, K.-E.; Jeon, H.-T.; Han, S.-Y.; Ham, J.; Kim, Y.-J.; Lee, S. W. *Dalton Trans.* **2009**, 6578−6592. (i) Callear, S. K.; Spencer, J.; Patel, H.; Deadman, J.; Hursthouse, M. B. *J. Chem. Crystallogr.* **2011**, *41* (4), 523−527.

(8) (a) Canty, A. J.; Honeyman, R. T. *J. Organomet. Chem.* **1990**, *387* (2), 247−263. (b) Canty, A. J.; Minchin, N. J. *J. Organomet. Chem.* **1982**, *226* (1), C14−C16. (c) Canty, A. J.; Minchin, N. J.; Patrick, J. M.; White, A. H. *J. Chem. Soc., Dalton Trans.* **1983**, 1253−1259.

(9) Zhao, S.-B.; Wang, R.-Y.; Wang, S. *J. Am. Chem. Soc.* **2007**, *129* (11), 3092−3093.

(10) Crosby, S. H.; Clarkson, G. J.; Rourke, J. P. *Organometallics* **2011**, *30* (13), 3603−3609.

(11) Butschke, B.; Schwarz, H. *Int. J. Mass Spectrom.* **2011**, *306* (2−3), 108−113.

(12) Butschke, B.; Schlangen, M.; Schröder, D.; Schwarz, H. *Int. J. Mass Spectrom.* **2009**, *283* (1−3), 3−8.

(13) Kwak, J.; Ohk, Y.; Jung, Y.; Chang, S. *J. Am. Chem. Soc.* **2012**, *134* (42), 17778−17788.

(14) Shibata, T.; Takayasu, S.; Yuzawa, S.; Otani, T. *Org. Lett.* **2012**, *14* (19), 5106−5109.

(15) Petretto, G. L.; Zucca, A.; Stoccoro, S.; Cinellu, M. A.; Minghetti, G. *J. Organomet. Chem.* **2010**, *695* (2), 256−259.

(16) (a) Zucca, A.; Petretto, G. L.; Stoccoro, S.; Cinellu, M. A.; Minghetti, G.; Manassero, M.; Manassero, C.; Male, L.; Albinati, A. *Organometallics* **2006**, *25* (9), 2253−2265. (b) Petretto, G. L.; Rourke, J. P.; Maidich, L.; Stoccoro, S.; Cinellu, M. A.; Minghetti, G.; Clarkson, G. J.; Zucca, A. *Organometallics* **2012**, *31* (8), 2971−2977.

(17) (a) Crabtree, R. H. *Coord. Chem. Rev.* **2013**, *257*, 755−766. (b) Iglesias, M.; Albrecht, M. *Dalton Trans.* **2010**, *39*, 5213−5215.

(18) For example, see Schuster, O.; Yang, L.; Raubenheimer, H. G.; Albrecht, M. *Chem. Rev.* **2009**, *109* (8), 3445−3478.

(19) Maidich, L.; Zuri, G.; Stoccoro, S.; Cinellu, M. A.; Masia, M.; Zucca, A. *Organometallics* **2013**, *32* (2), 438−448.

(20) (a) Constable, E. C.; Dunne, S. J.; Rees, D. G. F.; Schmitt, C. X. *Chem. Commun.* **1996**, 1169−1170. (b) Moorlag, C.; Clot, O.; Wolf, M. O.; Patrick, B. O. *Chem. Commun.* **2002**, 3028−3029. (c) Moorlag, C.; Wolf, M. O.; Bohne, C.; Patrick, B. O. *J. Am. Chem. Soc.* **2005**, *127* (17), 6382−6393.

(21) Zuber, M.; Pruchnik, F. P. *Polyhedron* **2006**, *25* (14), 2773−2777.

(22) For example, see (a) Stoccoro, S.; Chelucci, G.; Cinellu, M. A.; Zucca, A.; Minghetti, G. *J. Organomet. Chem.* **1993**, *450* (1−2), C15−C16. (b) Stoccoro, S.; Cinellu, M. A.; Zucca, A.; Minghetti, G.; Demartin, F. *Inorg. Chim. Acta* **1994**, *215* (1−2), 17−26. (c) Zucca, A.; Stoccoro, S.; Cinellu, M. A.; Minghetti, G.; Manassero, M.; Sansoni, M. *Eur. J. Inorg. Chem.* **2002**, *12*, 3336−3346.

(23) For example, see (a) Minghetti, G.; Doppiu, A.; Zucca, A.; Stoccoro, S.; Cinellu, M. A.; Manassero, M.; Sansoni, M. *Chem. Heterocycl. Compd.* **1999**, *8* (386), 1127−1137. (b) Doppiu, A.; Minghetti, G.; Cinellu, M. A.; Stoccoro, S.; Zucca, A.; Manassero, M. *Organometallics* **2001**, *20* (6), 1148−1152.

(24) Harris, C. M.; Kokot, S.; Patil, H. R. H.; Sinn, E.; Wong, H. *Aust. J. Chem.* **1972**, *25* (8), 1631−1643.

(25) Qaseer, H. A. *Croat. Chem. Acta.* **2005**, *78* (1), 79−84.

(26) Zaghal, M. H.; Qaseer, H. A. *Inorg. Chim. Acta* **1989**, *163* (2), 193−200.

(27) O'Connor, C. J.; Sinn, E. *Inorg. Chem.* **1978**, *17* (8), 2067−2071.

(28) Hoefelmeyer, J. D.; Schulte, M.; Tschinkl, M.; Gabbai, F. P. *Coord. Chem. Rev.* **2002**, *235*, 93−103.

(29) Hosmane, R. S.; Liebman, J. F. *Struct. Chem.* **2009**, *20*, 693−697.

(30) (a) Bonnington, K. J.; Zhang, F.; Moustafa, M. M. A. R.; Cooper, B. F. T.; Jennings, M. C.; Puddephatt, R. J. *Organometallics* **2011**, *31* (1), 306−317. (b) Johansson, L.; Tilset, M.; Labinger, J. A.; Bercaw, J. E. *J. Am. Chem. Soc.* **2000**, *122* (44), 10846−10855. (c) Romeo, R.; Plutino, M. R.; Elding, L. I. *Inorg. Chem.* **1997**, *36* (25), 5909−5916. (d) Zhong, H. A.; Labinger, J. A.; Bercaw, J. E. *J. Am. Chem. Soc.* **2002**, *124* (7), 1378−1399. (e) Alibrandi, G.; Minniti, D.; Romeo, R.; Uguagliati, P.; Calligaro, L.; Belluco, U. *Inorg. Chim. Acta* **1986**, *112* (2), L15−L16.

(31) (a) Peters, R. G.; White, S.; Roddick, D. M. *Organometallics* **1998**, *17* (20), 4493−4499. (b) Zhang, F.; Prokopchuk, E. M.; Broczkowski, M. E.; Jennings, M. C.; Puddephatt, R. J. *Organometallics* **2006**, *25* (7), 1583−1591. (c) Hickman, A. J.; Villalobos, J. M.; Sanford, M. S. *Organometallics* **2009**, *28* (18), 5316−5322. (d) Mazzone, G.; Russo, N.; Sicilia, E. *Inorg. Chem.* **2011**, *50* (20), 10091−10101. (e) Bercaw, J. E.; Chen, G. S.; Labinger, J. A.; Lin, B.-L. *Organometallics* **2010**, *29* (19), 4354−4359. (f) Guido, E.; D'Amico, G.; Russo, N.; Sicilia, E.; Rizzato, S.; Albinati, A.; Romeo, A.; Plutino, M. R.; Romeo, R. *Inorg. Chem.* **2011**, *50* (6), 2224−2239. (g) Kalberer, E. W.; Houlis, J. F.; Roddick, D. M. *Organometallics* **2004**, *23* (17), 4112−4115. (h) Stahl, S. S.; Labinger, J. A.; Bercaw, J. E. *J. Am. Chem. Soc.* **1996**, *118* (25), 5961−5976. (i) Heiberg, H.; Johansson, L.; Gropen, O.; Ryan, O. B.; Swang, O.; Tilset, M. *J. Am. Chem. Soc.* **2000**, *122* (44), 10831−10845. (j) Romeo, R.; D'Amico, G. *Organometallics* **2006**, *25* (14), 3435−3446. (k) Wik, B. J.; Lersch, M.; Tilset, M. *J. Am. Chem. Soc.* **2002**, *124* (41), 12116−12117.

(32) Eaborn, C.; Kundu, K.; Pidcock, A. *J. Chem. Soc., Dalton Trans.* **1981**, 933−938.

(33) Romeo, R.; Monsù Scolaro, L. *Inorg. Synth.* **1998**, *32*, 153.

(34) *Vogel's Textbook of Practical Organic Chemistry*, 5th ed.; Longman Scientific and Technical Ed.: Harlow, U.K., 1989.

(35) Granovsky, A. *Firefly*, version 7.1.G; www.http://classic.chem.msu.su/gran/firefly/index.html.

(36) Schmidt, M. W.; Baldridge, K. K.; Boatz, J. A.; Elbert, S. T.; Gordon, M. S.; Jensen, J. H.; Koseki, S.; Matsunaga, N.; Nguyen, K. A.; Su, S.; Windus, T. L.; Dupuis, M.; Montgomery, J. A. *J. Comput. Chem.* **1993**, *14* (11), 1347−1363.

(37) Perdew, J. P.; Burke, K.; Ernzerhof, M. *Phys. Rev. Lett.* **1996**, *77* (18), 3865−3868.

(38) Perdew, J. P.; Burke, K.; Ernzerhof, M. *Phys. Rev. Lett.* **1996**, *78* (7), 1396.

(39) Adamo, C.; Barone, V. *J. Chem. Phys.* **1999**, *110* (13), 6158−6169.

(40) Weigend, F.; Ahlrichs, R. *Phys. Chem. Chem. Phys.* **2005**, *7* (18), 3297−3305.

(41) Feller, D. *J. Comput. Chem.* **1996**, *17* (13), 1571−1586.

(42) Runge, E.; Gross, E. K. U. *Phys. Rev. Lett.* **1984**, *52* (12), 997−1000.

(43) Gross, E. K. U.; Kohn, W. *Phys. Rev. Lett.* **1985**, *55* (26), 2850−2852.

(44) (a) Azzena, U.; Chelucci, G.; Delogu, G.; Gladiali, S.; Marchetti, M.; Soccolini, F.; Botteghi, C. *Gazz. Chim. Ital.* **1986**, *116*, 307. (b) Botteghi, C.; Chelucci, G.; Chessa, G.; Delogu, G.; Gladiali, S.; Soccolini, F. *J. Organomet. Chem.* **1986**, *304* (1−2), 217−225.

(45) Smith, L. I.; Opie, J. W. *Org. Synth., Coll. Vol.* **1955**, *3*, 56; *Org. Synth.* **1948**, *28*, 11.

(46) Remarkably, at least in the case of **2b** and **2c**, grinding the sample in an agate mortar provoked partial degradation of the material.

(47) Coelho, A. A. *J. Appl. Crystallogr.* **2003**, *36*, 86−95.

(48) *TOPAS*, Version 3.0; Bruker AXS: Karlsruhe, Germany, 2005.

(49) Bönnemann, H. *Angew. Chem., Int. Ed. Engl.* **1978**, *17* (7), 505−515.

(50) Kaes, C.; Katz, A.; Hosseini, M. W. *Chem. Rev.* **2000**, *100* (10), 3553−3590.

(51) Butschke, B.; Schlangen, M.; Schröder, D.; Schwarz, H. *Chem.—Eur. J.* **2008**, *14* (35), 11050−11060.

(52) See, as an example, (a) Albrecht, M.; Stoeckli-Evans, H. *Chem. Commun.* **2005**, 4705−4707. (b) Poulain, A.; Neels, A.; Albrecht, M. *Eur. J. Inorg. Chem.* **2009**, *13*, 1871−1881.

(53) (a) Vicente, J.; Arcas, A.; Bautista, D.; Jones, P. J. *Organometallics* **1997**, *16* (10), 2127−2138. (b) Crespo, M.; Granell, J.; Solans, X.; Font-Bardia, M. *J. Organomet. Chem.* **2003**, *681* (1−2),

143−149. (c) Vicente, J.; Abad, J.-A.; Frankland, A. D.; Ramírez de Arellano, M. C. *Chem.—Eur. J.* **1999**, *5* (10), 3066−3075.
(54) Owen, J. S.; Labinger, J. A.; Bercaw, J. E. *J. Am. Chem. Soc.* **2004**, *126* (26), 8247−8255.
(55) Zucca A. et al., unpublished results.
(56) Pearson, R. G. *Inorg. Chem.* **1973**, *12* (3), 712−713.
(57) Janzen, D. A.; VanDerveer, D. G.; Mehne, L. F.; da Silva Filho, D. A.; Brédas, J.-L.; Grant, G. J. *Dalton Trans.* **2008**, *14*, 1872−1882.
(58) Ghedini, M.; Pugliese, T.; La Deda, M.; Godbert, N.; Aiello, I.; Amati, M.; Belviso, S.; Lelj, F.; Accorsi, G.; Barigelletti, F. *Dalton Trans.* **2008**, *32*, 4303−4318.
(59) Hallett, A. J.; Kariuki, B. M.; Pope, S. J. A. *Dalton Trans.* **2011**, *40*, 9474−9481.
(60) Bercaw, J. E.; Chen, G. S.; Labinger, J. A.; Lin, B.-L. *Organometallics* **2010**, *29* (19), 4354−4359.
(61) (a) Romeo, R.; Fenech, L.; Monsù Scolaro, L.; Albinati, A.; Macchioni, A.; Zuccaccia, C. *Inorg. Chem.* **2001**, *40* (14), 3293−3302. (b) Romeo, R.; Fenech, L.; Carnabuci, S.; Plutino, M. R.; Romeo, A. *Inorg. Chem.* **2002**, *41* (11), 2839−2847. (c) Romeo, R.; Carnabuci, S.; Plutino, M. R.; Romeo, A.; Rizzato, S.; Albinati, A. *Inorg. Chem.* **2005**, *44* (5), 1248−1262. (d) Romeo, R.; Carnabuci, S.; Fenech, L.; Plutino, M. R.; Albinati, A. *Angew. Chem., Int. Ed.* **2006**, *45*, 4494−4498. (e) Romeo, R.; D'Amico, G.; Guido, E.; Albinati, A.; Rizzato, S. *Inorg. Chem.* **2007**, *46* (25), 10681−10692.
(62) For example, see (a) Lersch, M.; Tilset, M. *Chem. Rev.* **2005**, *105*, 2471−2526. (b) Johansson, L.; Tilset, M.; Labinger, J. A.; Bercaw, J. E. *J. Am. Chem. Soc.* **2000**, *122*, 10846−10855. (c) Johansson, L.; Tilset, M. *J. Am. Chem. Soc.* **2001**, *123*, 739−740. (d) Johansson, L.; Ryan, O. B.; Rømming, C.; Tilset, M. *J. Am. Chem. Soc.* **2001**, *123*, 6579−6590. (e) Zhong, H. A.; Labinger, J. A.; Bercaw, J. E. *J. Am. Chem. Soc.* **2002**, *124*, 1378−1399.
(63) Crabtree, R. H. *Science* **2010**, *293*, 455−456.
(64) Hashiguchi, B. G.; Young, K. J. H.; Yousufuddin, M.; Goddard, W. A.; Periana, R. A. *J. Am. Chem. Soc.* **2010**, *132* (36), 12542−12545.
(65) Koo, C.-K.; Lam, B.; Leung, S.-K.; Lam, M. H.-W.; Wong, W.-Y. *J. Am. Chem. Soc.* **2006**, *128* (51), 16434−16435.